

REFERENCES

- Amash, A. and Zugenmaier, P. (1998). Study on cellulose and xylan filled polypropylene composites. Polymer Bulletin, 40(2–3), 251.
- Bataille, P., Ricard, L. and Sapieha, S. (1989). Effects of cellulose fibers in polypropylene composites. Polymer Composites, 10(2), 103–108.
- Beckermann, G.W. and Pickering, K.L. (2008). Engineering and evaluation of hemp fibre reinforced polypropylene composites: Fibre treatment and matrix modification. Composites: Part A, 39, 979–988.
- Belgacem, M. N. and Gandini, A. (2005). The surface modification of cellulose fibres for use as reinforcing elements in composite materials. Composite Interface, 12(1–2), 41–75.
- Bledzki, A. K. and Gassan, J. (1999). Composites reinforced with cellulose based fibers. Progress in Polymer Science, 24, 221–274.
- Bledzki, A. K., Reihmane, S. and Gassan, J. (1996). Properties and modification methods for vegetable fibres for natural fibres composites. Journal of Applied Polymer Science, 59(8), 1329–1336.
- Botaro, V. R. and Gandini, A. (1998). Chemical modification of the surface of cellulose fibres. 2. Introduction of alkenyl moieties via condensation reactions involving isocyanate functions. Cellulose, 5(2), 65.
- Canche, E.G., Rodri, G.T.G., Herrera, F.P.J., Mendiza, B.E. and Puig, J.E. (1997). Preparation and characterization of henequen cellulose grafted with methyl methacrylate and its application in composites. Journal of Applied Polymer Science, 66 339–346.
- Carvalho, A.J.F., Curvelo, A.A.S. and Gandini, A. (2005). Surface chemical modification of thermoplastic starch: reactions with isocyanates, epoxy functions and stearoyl chloride. Industrial Crops and Products, 21, 331–336.
- Chakraborty, A., Sain, M. and Kortschot, M. (2006). Cellulose microfibrils as reinforcing agents for structural materials. ACS Symposium Series, 938, 169–186.

- Corrales, F., Llop, M., Mutje, P., Vilaseca, F. and Gandini, A. (2002). Jute fibers esterification to improve the adhesion with the matrix in reinforced polymers. Iberoamerican Congress on Pulp and Paper Research.
- Corrales, F., Vilaseca, F., Llop, M., Girones, J., Mendez, J.A. and Mutje, P. (2007). Chemical modification of jute fibers for the production of green composites. Journal of Hazardous Materials, 144, 730–735.
- Cruz, R. A., Mendoza, A. M., Vieira, M. C. and T.Heinze. (1999). Studies on grafting of cellulosic,aterials isolated from Agave lechuguilla and fourcroydes. Die Angewandte Makromolekulare Chemie, 273, 86–90.
- Das, A., Saikia, C. N. and Hussain, S. (2001). Grafting of methyl methacrylate (MMA) onto Antheraea assama silk fiber. Journal of Applied Polymer Science, 81, 2633–2641.
- Dong, S., Sapieha, S. and Schreiber, H. P. (1993). Mechanical properties of corona–modified cellulose/polyethylene composites. Polymer Engineering and Science, 33(6), 343–346.
- Drzal, L. T., Mohanty, A. K. and Misra, M. (2003). Structural biocomposites from natural fibres and biopolymers. Annual Technical Conference – ANTEC, 2, 2024–2028.
- Espart, A., Camacho, W. and Karlson, S. (2003). Thermal and thermomechanical properties of biocomposites made from modified recycled cellulose and recycled polypropylene. Journal of Applied Polymer Science, 89, 2353–2360.
- Felix, J. M. and Gatenholm, P. (1991). Effect of compatibilizing agents on the interfacial strength in cellulose–polypropylene composites. Polymeric Materials Science and Engineering, 42, 609–620.
- Gassan, J. and Bledzki, A. K. (1997). The influence of fiber–surface treatment on the mechanical properties of jute–polypropylene composites. Composite Part A, 28A(12), 1001–1005.
- Gassan, J. and Bledzki, A. K. (2000). Possibilities to improve the properties of natural fibre plastics by fibre modification – jute polypropylene composites. Journal of Applied Polymer Science, 7(5–6), 373–385.

- George, J., Sreekala, M. S. and Thomas, S. (2001). A review on interface modification and characterization of natural fibre reinforced plastic composites. Polymer Engineering and Science, 41(9), 1471–1485.
- Joly, C., Gauthier, R. and Escoubes, M. (1996). Partial masking of cellulosic fiber hydrophilicity for composite applications. Water sorption by chemically modified fibers. Journal of Applied Polymer Science, 61(1), 57–69.
- Karmarkar, A., Chauhan, S.S., Modak, J.M., Chanda, M. (2007). Mechanical properties of wood-fiber reinforced polypropylene composites: Effect of a novel compatibilizer with isocyanate functional group. Composites Part A: Applied Science and Manufacturing, 38(2), 227–233.
- Khullar, R., Varshney, V. K., Naithani, S. and Soni, P. L. (2008). Grafting of acrylonitrile onto cellulosic material derived from bamboo (*Dendrocalamus strictus*). eXPRESS Polymer Letters, 2(1), 12–18.
- Lee, S. M. (1990). International Encyclopedia of Composites. New York: VCH, 2.
- Loria, B.M.I., Carrilo, E.H.J. and Aguilar, V.M.J. (2002). Grafting of poly(acrylic acid) onto cellulosic microfibers and continuous cellulose filaments and characterization. Journal of Applied Polymer Science, 83, 386–393.
- Lu, J., Askeland, P. and Lawrence T.D. (2008). Surface modification of microfibrillated cellulose for epoxy composite applications. Polymer, 49, 1285–1296.
- Ly, B., Dufresne, A., Chaussy, D. and Belgacem, M.N. (2008). Surface functionalization of cellulose fibres and their incorporation in renewable polymeric matrices. Composites Science and Technology, 68, 3193–3201.
- Mishra, S., Misra, M., Tripathy, S. S., Nayak, S. K. and Mohanty, A. K. (2002). The influence of chemical modification on the performance of sisal–polyester biocomposites. Polymer Composites, 23(2), 164–170.
- Mohanty, A. K., Misra, M. and Drzal, L. T. (2001). Surface modification of natural fibers and performance of the resulting biocomposites: An overview. Composite Interface, 8(5), 313–343.

- Mohanty, A. K., Tripathy, P. C., Misra, M., Parija, S. and Sahoo, S. (2000). Chemical modification of pineapple leaf fiber: graft copolymerization of acrylonitrile onto defatted pineapple leaf fibers. Journal of Applied Polymer Science, 77(14), 3035–3043.
- Nowrbakhsh, A., Kokta, B.V., Alireza, A. and Ahmad, J.L. (2008). Effect of a novel coupling agent, polybutadiene isocyanate, on mechanical properties of wood-fiber polypropylene composites. Journal of Reinforced Plastics and Composites, 27, 16–17.
- Oksman, K., Mathew, A. P., Bondeson, D. and Kvien, I. (2006). Manufacturing process of cellulose whiskers/polylactic acid nanocomposites. Composites Science and Technology, 66(15), 2776–2784.
- Oujai, S., Hodzic, A. and Shanks, R.A. (2004). Morphology and grafting modification of natural cellulose fibers. Journal of Applied Polymer Science, 94, 2456–2465.
- Panaitescu, D. M., Donescu, D., Bercu, C., Vuluga, D. M., Iorga, M. and Ghiurea, M. (2007). Polymer composites with cellulose microfibrils. Polymer Engineering and Science, 47(8), 1228–1234.
- Pasquini, D., Texeira, E.M. and Curvelo, A.A.S. (2008). Surface esterification of cellulose fibers: Processing and characterization of low-density PE/cellulose fibers composites. Composites Science and Technology, 68, 193–201.
- Qing, L. and Laurent M.M. (2003). Surface of cellulosic materials modified with functionalized polyethylene coupling agents. Journal of Applied Polymer Science, 88, 278–286.
- Qiu, W., Endo, T. and Hirotsu, T. (2006). Structure and properties of composites of highly crystalline cellulose with polypropylene: Effects of polypropylene molecular weight. European Polymer Journal, 42(5), 1059–1068.
- Randell, D. and Steve, L. (2002). The Polyurethane Book, New York: Wiley.
- Razaina, M. T. (1998). Cellulose fiber-reinforce thermoplastic composites: Processing and product characteristics. Master of Science in Wood Science and Forest Products, Master, Blacksburg, Virginia.

- Rensch, H. P. and Riedl, B. (1992). Characterization of chemically modified chemi-thermomechanical pulp by thermal analysis. Part 2. Treatment with isocyanates. Thermochimica Acta, 210(171–183).
- Rogovin, Z. A. (1972). Several problems in the synthesis of graft copolymers of cellulose and in investigating their properties. Journal of Polymer Science, 37, 221–237.
- Rowell, R. M. (2002). Sustainable composites from natural resources. High Performance Structures and Materials, 4, 183–192.
- Sain, M., Suhara, P., Law, S. and Bouilloux, A. (2005). Interface modification and mechanical properties of natural fiber-polyolefin composite. Journal of Reinforced Plastics and Composites, 24(2), 121–130.
- Sanadi, A. R., Young, R. A., Clemons, C. and Rowell, R. M. (1994). Recycled newspaper fibers as reinforcing fillers in thermoplastics: Part I. Analysis of tensile and impact properties in polypropylene. Journal of Reinforced Plastics and Composites, 13(1), 54–67.
- Sapieha, S., Bataille, P. and Dufourd, M. (1991). Graft copolymerization of styrene onto cellulose by corona discharge. American Chemical Society, Polymer Preprints, Division of Polymer Chemistry, 32(1), 559–560.
- Stenstad, P., Andresen, M., Tanem, B. S. and Stenius, P. (2008). Chemical surface modification of microfibrillated cellulose. Cellulose, 15, 35–45.
- Takacs, E., Wojnarovits, L., Borsa, J., Foldvary, C., Hargittai, P. and Zold, O. (1999). Effect of γ -irradiation on cotton-cellulose. Radiation Physics and Chemistry, 55(5), 663–666.
- Thompson, T. T., Bastarrachea, M. I. L. and Vega, M. J. A. (2005). Studies on lignocellulosic fibers of Brazil: Part III – Morphology and properties of Brazilian curaua fibers. Composites: Part A, 38, 2227–2236.
- Tomezek, F., Kestur, G.S. and Thais, H.D. (2008). Characterization of henequen cellulose microfibers treated with an epoxide with poly(acrylic acid). Carbohydrate Polymers, 62, 67–73.

- Vaibhao, J., Huining, X. and Yonghao, N. (2007). Grafting of poly(methyl acrylate) onto sulfite pulp fibers and its effect on water absorbance. Journal of Applied Polymer Science, 105, 3195–3203.
- Wulin, Q., Farao, Z., Endo, T. and Hirotsu, T. (2005). Isocyanate as a compatibilizing agent on the properties of highly crystalline cellulose/polypropylene composites. Journal of Materials Science, 40, 3607–3614.
- Yan, L., Yanping, H., Chunjing, H. and Yehong, Y. (2008). Microstructure and mechanical properties of natural fibres. Advanced Materials Research, 33–37(Part 1), 553–558.
- Yano, H., Nakagaito, N. A., Ifuku, S., Iwamoto, S. I., Nogi, M. and Abe, K. (2006). Bio–nanocomposites. Polymer Preprints, Japan, 55(2), 5116–5117.

APPENDICES

APPENDIX A In situ atom transfer radical polymerization (ATRP) of butyl acrylate in an attempt to render the surface of cellulose fiber hydrophobic

APPENDIX B Enhancement of the Paper Performance

APPENDIX C BET Results

APPENDIX A

In situ atom transfer radical polymerization (ATRP) of butyl acrylate in an attempt to render the surface of cellulose fiber hydrophobic

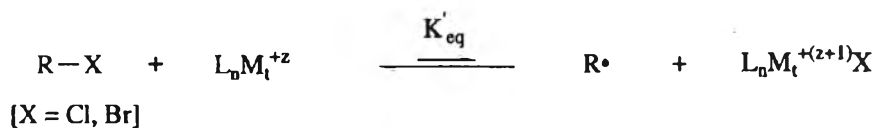
INTRODUCTION

This work was done with the cooperation of Mr. Shuzhao Li from The School of Materials Science and Engineering, East China University of Science and Technology, Shanghai, China. In order to compare the products performance, ATRP was studied.

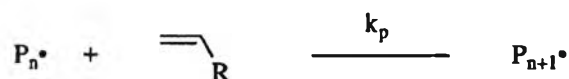
Atom Transfer Radical Polymerization (ATRP) is a controlled/living polymerization based on the use of radical polymerization to convert monomer to polymer. Since radical polymerization can polymerize hundred monomers, can copolymerize two or more monomers, and can be performed in water as emulsions or suspension, so the controlling radical polymerization can promise~~x~~ to overcome these limitation and provide a method to maximize the potential of living polymerization. The control over radical polymerizations is based on two principles. First, initiation should be fast, providing a constant concentration of growing polymer chains. Secondly, because of the persistent effect, the majority of these growing polymer chains are dormant species that still preserve the ability to grow because a dynamic equilibrium between dormant species and growing radical is established.

ATRP is a free-radical induced polymerization process that used a transition metal in combination with a suitable ligand as a catalyst. The complex catalyst establishes a reversible equilibrium between growing radicals and dormant species, the mechanism of ATRP is shown in Figure A.1. The equilibrium is attenuated by the choice of the ligand and this ligand also increases the solubility of the complex catalyst in the polymerization medium.

Initiation:



Propagation:



Termination:

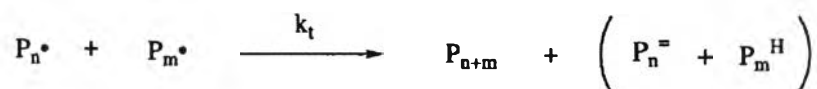


Figure A.1 The mechanism of Atom Transfer Radical Polymerization (ATRP).

The kinetic chain length of a radical polymerization is proportional to the ratios of the monomer-to-radical concentrations and of the propagation-to-termination rate constants. Thus, it seems that with a controlled free radical polymerization it would be possible only to prepare a small concentration of polymer chains of a very high molecular weight (Patten T.E. *et al.* 1998).

As a multicomponent system, ATRP is composed of the monomer, an initiator with a transferable (pseudo)halogen, and a catalyst (consisted of a transition metal species with any suitable ligand).

A.1 ATRP of Various Monomers

A variety of monomers have been successfully polymerized using ATRP including styrenes, acrylates, methacrylates, acrylonitriles, and meth(acrylamides). Even under the same conditions using the same catalyst, each monomer has its own

unique atom transfer equilibrium constant for its active and dormant species. In the absence of any side reactions other than radical termination by coupling or disproportionation, the magnitude of the equilibrium constant ($K_{eq} = k_{act}/k_{deact}$) determines the polymerization rate. ATRP will not occur or occur very slowly if the equilibrium constant is too small. In contrast, too large an equilibrium constant will lead to a large amount of termination because of a high radical concentration. This will be accompanied by a large amount of deactivating higher oxidation state metal complex; which will shift the equilibrium toward dormant species and may result in the apparently slower polymerization (Queffelec J. *et al.* 2000). Each monomer possesses its own intrinsic radical propagation rate. Thus, for a specific monomer, the concentration of propagating radicals and the rate of radical deactivation and the optimal conditions for polymerization which include concentration and type of the catalyst, temperature, solvent, and some additives need to be adjusted to maintain polymerization control. However, since ATRP is a catalytic process, the overall position of the equilibrium not only depends on the radical (monomer) and the dormant species, but also can be adjusted by the amount and reactivity of the transition-metal catalyst added.

A.1.1 Styrene

ATRP of styrene and its derivatives has been reported for the copper (Percec V. *et al.* 1995; Patten T.E. *et al.* 1998), iron (Wei M. *et al.* 1997), ruthenium (Kotani Y. *et al.* 2000), and rhenium (Kotani Y. *et al.* 1999) catalytic systems; thus far the majority of the work has been performed using the copper-based systems. One of the most extensively studied systems is the polymerization of styrene conducted at 110°C with CuBr(dNbpy)₂ as the catalyst and alkyl bromides as the initiators. A similar system for the chloride-mediated polymerization is conducted at 130°C to obtain similar polymerization rates (Patten T.E. *et al.* 1998). The reaction temperature can be lowered to 80-90°C to produce well-defined polystyrenes in a reasonable time with the use of a more efficient catalyst, such as CuBr/PMDETA (*N,N,N',N'',N''*-penta methyldiethylenetriamine) (Xia J. *et al.* 1997) or CuOAc/CuBr/dNbpy (Matyjaszewski K. *et al.* 1998). However, to maintain a sufficiently large propagation rate, avoid vitrification at high conversion (for polystyrene T_g 100°C), and sometimes increasing the solubility of the catalysts, higher reaction temperatures (>100°C), are preferred for styrene ATRP. The reaction may be carried out in bulk or using a sol-

vent, but the stability of the halide end group displays a pronounced solvent dependence as demonstrated by model studies using 1-phenylethyl bromide. As a result, non-polar solvents are recommended for styrene ATRP (Matyjaszewski K. *et al.* 1997). Figure A.2 shows some styrene derivatives successfully polymerized by ATRP.

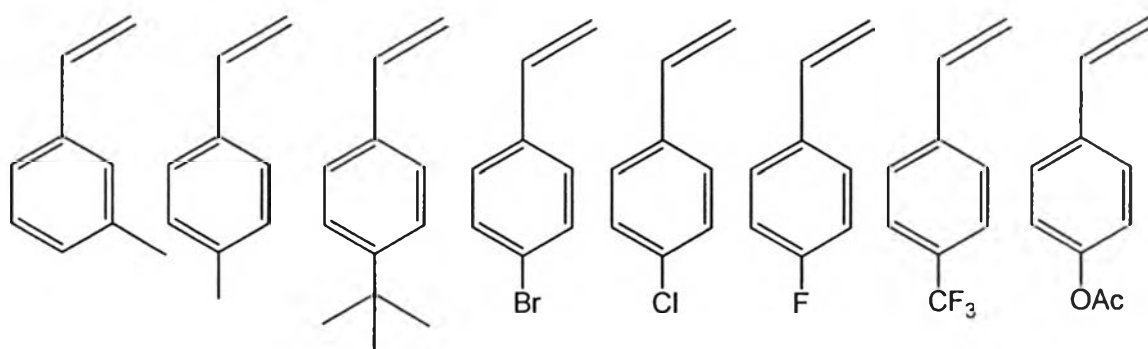


Figure A.2 Various styrene derivatives polymerized by ATRP.

A.1.2 Acrylate

The controlled ATRP of acrylate has been reported for copper- (Wang J.S. *et al.* 1995; Wang J.S. *et al.* 1995; Davis K.A. *et al.* 1999), ruthenium- (Simal F. *et al.* 1999), and iron-based systems (Teodorescu M. *et al.* 2000). Copper appears to be superior over other transition metals in producing well-defined polyacrylates with low polydispersities in a relatively short time. Typically polymerizations were conducted in bulk with an alkyl 2-bromopropionate initiator. Depending on the catalyst, a wide range of polymerization temperatures are possible to produce polymers within a reasonable time. A wide range of acrylates with various side chains have been polymerized using ATRP (Figure A.3). When allyl acrylate was subjected to ATRP conditions with bpy or dNbpy as the ligand, a cross-linking reaction occurred, even at 0°C (Matyjaszewski K. 1998).

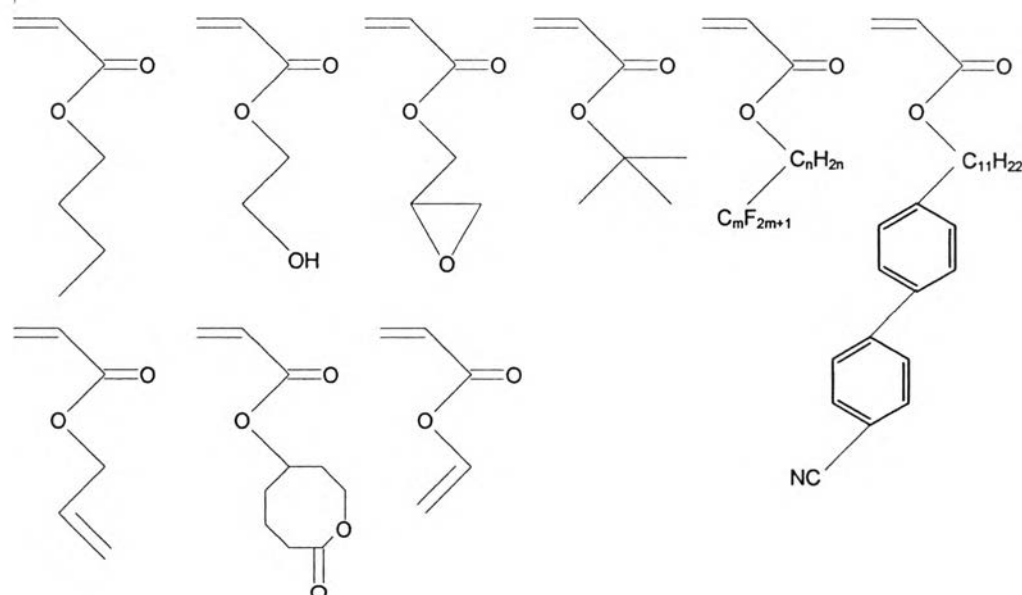


Figure A.3 Various acrylate derivatives polymerized by ATRP.

Liu P. *et al.* (2005) were successfully grafted poly(*n*-butyl acrylate) with starch (PBA-g-Starch) by the surface-initiated atom transfer radical polymerization (SI-ATRP) of *n*-butyl acrylate (BA) using starch bromo-acetic ester as macroinitiator in presence of 1,10-phenanthroline and Cu(I)Br as catalyst in toluene system for the first time, the preparation of the grafted of this macroinitiator and the mechanism of SI-ATRP of BA from the surface of starch are shown in Figure A.3 and A.4 ,respectively.

Because of the distinct difference of carbon element contents between the starch (44.44%) and PBA (61.54%), it is possible to calculate the grafting parameters such as C% and PG% from the elemental analyses, the conversion of the monomer (C%) and the percentage of grafting (PG%) calculation are shown in the following equations.

$$C\% = \frac{\text{PBA grafted (g)}}{\text{Monomer used (g)}} \times 100\%$$

$$PG\% = \frac{\text{PBA grafted (g)}}{\text{Starch charged (g)}} \times 100\%$$

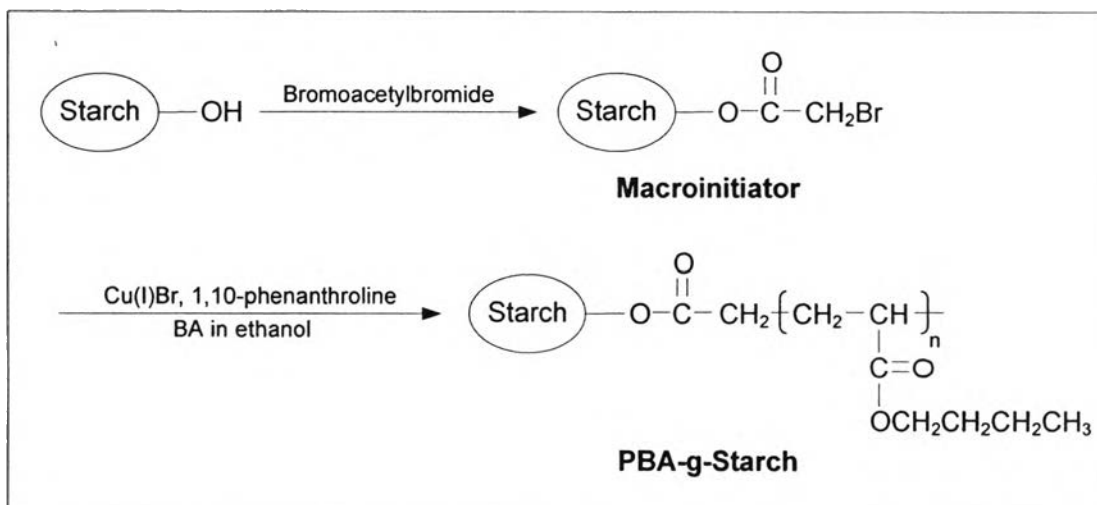


Figure A.4 Preparation route to the PBA-g-Starch.

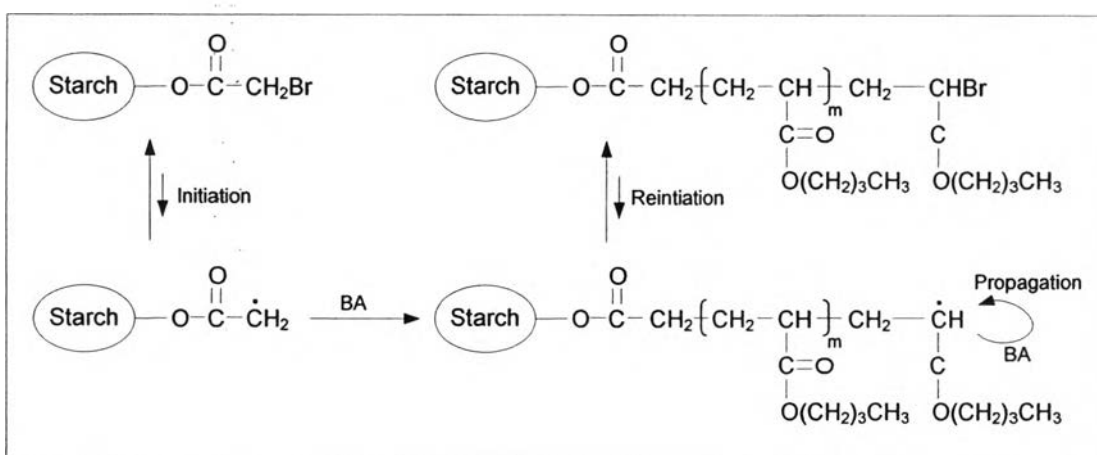


Figure A.5 The mechanism of the SI-ATRP of BA.

It was found that the C% and PG% increased to 9.9 and 21.3%, respectively, with the increasing of the polymerizing time, as shown in Figure A.6. As can be seen, there is a linear increase in the C% and PG% with the increasing of the polymerizing time. This exhibited the characteristics of a controlled/'living' polymerization. At higher C%, the results start to spread. This might result from the wrapping of some initiator groups.

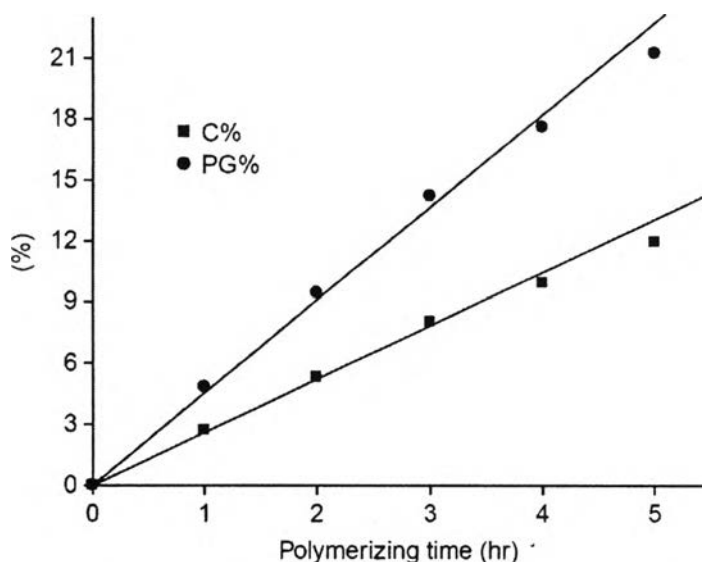


Figure A.6 The effect of the polymerizing time on the C% and PG%.

They have been found a glass transition temperature (T_g) of the PBA-g-Starch after a polymerizing time of 5 h which was -48.6°C by the differential scanning calorimetry (DSC) analysis. The product was also characterized by Fourier transform infrared (FTIR) and X-ray diffraction (XRD) techniques.

A.1.3 Methacrylate

ATRP of methyl methacrylate (MMA), Figure A.7, has been reported for copper, nickel, iron, and rhodium catalytic systems. The facile polymerizability of MMA and the large range of available catalysts for the ATRP reaction are due to the relative ease of activation of the dormant species and the high values of the ATRP equilibrium constants. Most polymerizations of MMA were carried out in solution at temperatures ranging from 70 to 90°C . In addition, solution polymerization helps to keep the concentration of growing radicals low. Under comparable conditions, the copper-mediated ATRP of MMA displays a significantly higher equilibrium constant when compared with styrene and MA.

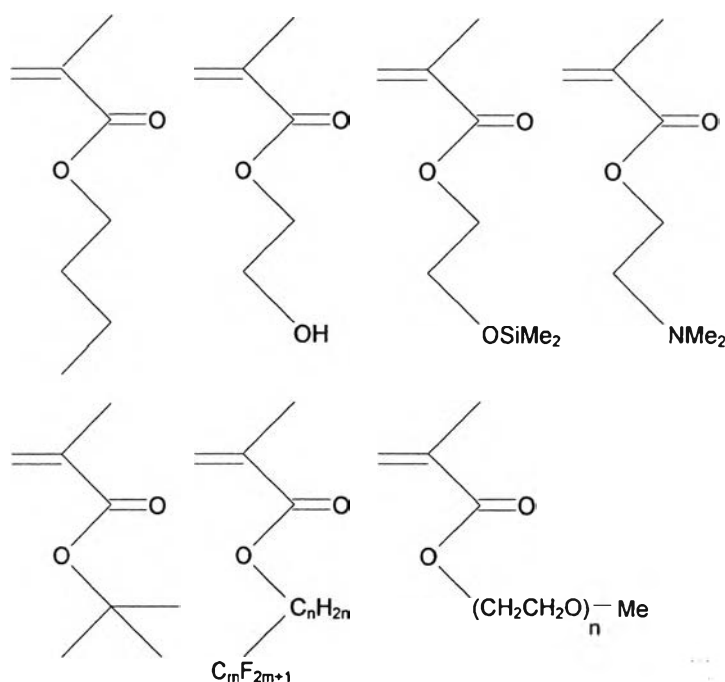


Figure A.7 Various methacrylate derivatives polymerized by ATRP.

Nurmi L. *et al.* (2007) polymerized the graft copolymers of acetylated starch oligomer (AS) and poly(methyl methacrylate) (PMMA) by atom transfer radical polymerization (ATRP) with used 2-bromo-isobutyryl-bromide (BIB) as a macroinitiator. AS was converted to an ATRP macroinitiator by converted a part of the hydroxyl groups of AS to 2-bromoisobutyryl groups. Prepared macroinitiators by vary degrees of substitution for the 2-bromoisobutyryl group. The polymerizations were conducted using Copper (I) Bromide (CuBr)/2,2-bipyridine (BiPy) catalyst system, either in bulk or in 1:1 v/v Tetrahydrofuran (THF) solution. They proceeded with first-order kinetics and the molecular weights of the polymers increased linearly with conversion. Graft copolymers with different graft densities and graft lengths were prepared in a controlled manner. The hydrophobicity of these copolymers was studied by contact angle measurements.

A series of ATRP macroinitiators was produced by functionalization of AS. A part of the hydroxyl groups of AS were replaced with 2-bromo-isobutyryl groups, which are able to initiate polymerization by the ATRP mechanism. Three different

macroinitiators (AS–BIB1, AS–BIB2, AS–BIB3) were prepared with different degrees of substitution for the initiator group. The degree of substitution (DS) is defined as the number of hydroxyl groups per anhydroglucose unit, which have been substituted by other groups. Since anhydroglucose units contain originally three hydroxyl groups, the maximum possible DS is three. However, since AS used in this study already contained acetyl groups with DS of 2.2, the maximum DS for the initiator groups (DS_{ini}) was 0.8.

Macroinitiators were prepared by adding different amounts of BIB relative to the amount of hydroxyl groups of AS to the reaction. The macroinitiators are presented in Table A.1. They enabled grafting with low (DS_{ini} 0.02), intermediate (DS_{ini} 0.09) and high (DS_{ini} 0.76) grafting density. The achieved degrees of substitution correspond to 51.4, 10.5 and 1.3 anhydroglucose units per initiating site, respectively. One may notice that with AS–BIB3 approximately all remaining hydroxyl groups of AS have been converted to initiating sites.

Table A.1 Macro-initiators

Macroinitiator	Mole ratio in reaction ^a	Degree of substitution ^b (¹³ C NMR)	Apparent M_n^c (SEC) g/mol
AS–BIB1	0.3	0.02	5900
AS–BIB2	1	0.09	7000
AS–BIB3	3.9	0.76	11,600

^a Mole ratio of BIB/OH groups in reaction mixture.

^b The amount of 2–bromo–isobutyryl groups/AS anhydroglucose unit.

^c Determined with respect to linear polystyrene standards.

DS_{ini} was determined by ¹³C NMR spectroscopy. The ¹³C NMR spectrum of macroinitiator AS–BIB3 is presented in Figure A.8. The intensity of the acetyl group CH₃ carbon peak (9,10 in the figure) was compared with the intensity 2-bromo-

isobutyryl group CH_3 carbon peak (12 in the figure). The DS_{ini} and hence also the graft density in polymerization could easily be tuned by changing the ratio of BIB relative to OH groups in the reaction.

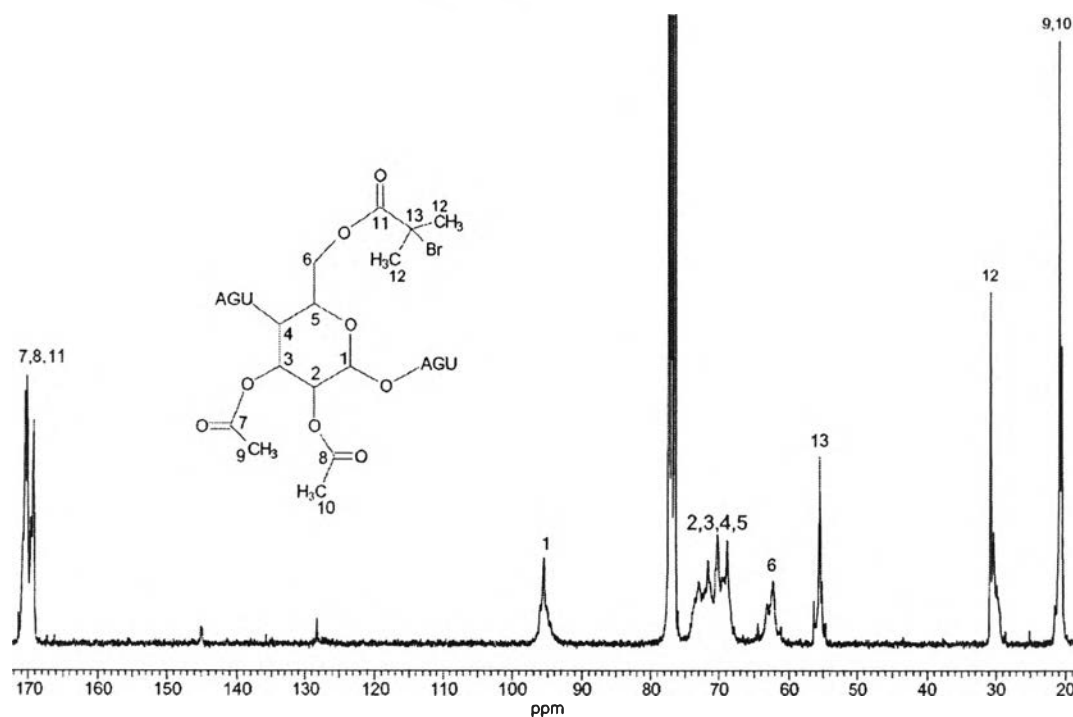


Figure A.8 300 MHz ^{13}C NMR spectrum of AS macroinitiator (AS-BIB3) with assigned peaks.

A.1.4 Acrylonitrile

Metal mediated controlled radical polymerization of acrylonitrile has so far been reported for copper-mediated ATRP (Matyjaszewski K. *et al.* 1999; Matyjaszewski K. *et al.* 1997; Jo S.M. *et al.* 1996). DMF is a good solvent for polyacrylonitrile, however, it may also complex with copper and deactivate the catalyst (Matyjaszewski K. *et al.* 2001).

A.2 Initiator

The main role of the initiator is to determine the number of growing polymer chains. The theoretical molecular weight or degree of polymerization (DP) increases reciprocally with the initial concentration of initiator in a living polymerization as shown in the following equation (Matyjaszewski K. *et al.* 2001):

$$DP = \frac{[M]_0}{[\text{Initiator}]_0} \times \text{Conversion}$$

In ATRP reaction, alkyl halides (RX) are typically used as the initiator and the rate of the polymerization is first order with respect to the concentration of RX. To obtain well-defined polymers with narrow molecular weight distributions, the halide groups (X) must rapidly and selectively migrate between the growing chain and the transition-metal complex. Thus far, when X is either bromine or chlorine, the molecular weight control is the best. The initiation should be fast and quantitative with a good initiator. In general, any alkyl halide with activating substituents on the α -carbon, such as aryl, carbonyl, or allyl groups, can potentially be used as ATRP initiators.

As discussed previously, the amount of the initiator in the ATRP determines the final molecular weight of the polymer at full monomer conversion. Multifunctional initiators may provide chain growth in several directions. Fast initiation is important to obtain well-defined polymers with low polydispersities. A variety of initiators, typically alkyl halides, have been used successfully in ATRP. Many different types of halogenated compounds are potential initiators.

A.2.1 Halogenated alkane

Halogenated alkanes, such as CHCl_3 or CCl_4 , are typically used in atom transfer radical addition and were among the first studied as ATRP initiators (Wang J.S. *et al.* 1995; Kato M. *et al.* 1995). CCl_4 has also been used in other catalytic systems, including the Cu-based (Wang J.S. 1995). When $\text{CuCl}(\text{bpy})_3$ was used as the catalyst for the ATRP of styrene at 130°C , CCl_4 was found to act as a bifunctional initiator (Destarac M. *et al.* 2000).

A.2.2 Benzylic halides

Benzylic-substituted halides are useful initiators for the polymerization of styrene and its derivatives due to their structural resemblance. However, they fail in the polymerization of more reactive monomers in ATRP such as MMA. Figure A.9 illustrates some examples of halogenated alkanes and benzylic halides used successfully in ATRP.

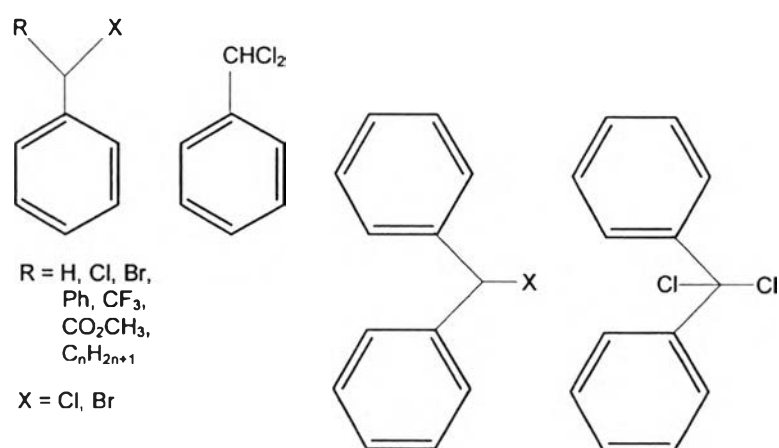


Figure A.9 Some halogenated alkanes and benzylic halides used as ATRP initiators.

A.2.3 Sulfonyl halide

As ATRP initiators, sulfonyl chlorides yield a much faster rate of initiation than monomer propagation (Percec V. *et al.* 1998). A unique feature of the sulfonyl halides as initiators is that although they are easily generated, they only dimerize slowly to form disulfones and slowly disproportionate. Thus, they can react with the monomers and initiate the polymerization efficiently.

In the summary of the initiator characteristic, two parameters are important for a successful ATRP initiating system. First, initiation should be fast in comparison with propagation. Second, the probability of side reactions should be minimized.

The basic requirement for a good ATRP initiator is that it should have reactivity at least comparable to that of the subsequently formed growing chains. This also indicates that not all initiators are good for all monomers. This is an important

criterion for the preparation of block copolymers. Very reactive initiators may produce too many radicals, which will terminate at early stages. This will reduce efficiency of initiation, too much of the deactivator production, and slow process. It is necessary to better correlate structures of the alkyl halides with their ATRP reactivities. This includes both the alkyl part (electronic and steric effects) and (pseudo)halogens part. The structure reactivity correlation should include both components as well as the effects of solvent and temperature. Halogen end groups are an inherent part of the ATRP systems. They can be replaced by many synthetic methods to provide more useful functionalities and provide halogen-free products.

A.3 Transition metal (Catalyst)

The most important component of ATRP is the catalyst. It is the key to ATRP since it determines the position of the atom transfer equilibrium and the dynamics of exchange between the dormant and active species. In order to generate the growing radicals, the metal center should undergo an electron transfer reaction with the abstraction of a (pseudo)halogen and expansion of the coordination sphere. The oxidized transition metal should rapidly deactivate the propagating polymer chains to form the dormant species.

There are several requirements for an effective ATRP catalyst. First, the metal complex must have an accessible one-electron redox couple to promote atom transfer, but this requirement alone is not sufficient, because as its name indicates ATRP is an atom transfer not an electron transfer process. Therefore, a second requirement is that upon one electron oxidation, the coordination number of the metal center must increase by one in order to accommodate a new ligand. A third requirement for a good ATRP catalyst is that the catalyst must show selectivity for atom transfer and therefore possess a low affinity for alkyl radicals and the hydrogen atoms on alkyl groups. Finally, the metal center must not be a strong Lewis acid; otherwise the ionization of certain initiators/end groups to carbocations may occur (Patten T.E. *et al.* 1998).

Copper catalysts are superior in ATRP in terms of versatility and cost. Styrenes, (meth)acrylate esters and amides, and acrylonitrile have been successfully polymerized using copper-mediated ATRP. The first copper-based ATRP system was

reported in 1995. Controlled polymerizations with a linear increase of the molecular weight with conversion were achieved for styrene, MA, and MMA.

Wang J.S. *et al.* (1995) reported the results of the ATRP by using a simple alkyl halide, R-X (X = Cl and Br), as an initiator and a transition metal species complexed by suitable ligand(s), CuX/2,2'-bipyridine, as a catalyst, ATRP of vinyl monomers such as styrene and (meth)acrylate proceeded in a living fashion with a constant complexing ligand/catalyst/initiator molar ratio of 3/1/1, yielding polymers with degrees of polymerization predetermined by $\Delta[M]/[I]_0$ up to $M_n \approx 10^5$ and low polydispersities, $1.1 < M_w/M_n < 1.5$.

A.4 Ligand

The main role of the ligand in ATRP is to solubilize the transition-metal salt in the organic media and to adjust the redox potential of the metal center for appropriate reactivity and dynamics for the atom transfer (Xia J. *et al.* 2000). Ligands serve several purposes. In addition, they control the solubility in the reaction mixture and ensure stability of the complexes in different monomers, solvents, and temperatures. Ligands may also facilitate the removal and recycling of the catalyst. They may allow the immobilization of the catalyst and also distribution between two phases.

A.4.1 Nitrogen Ligand

Nitrogen ligands have been used in copper- and iron-mediated ATRP. For copper-mediated ATRP, nitrogen-based ligands work particularly well. In contrast, sulfur, oxygen, or phosphorus ligands are less effective due to inappropriate electronic effects or unfavorable binding constants. For copper-based ATRP, the coordination chemistry of the transition-metal complex greatly affects the catalyst activity. A recent survey summarized different ligands employed in copper-mediated ATRP. Activity of N-based ligands in ATRP decreases with the number of coordinating sites: $N_4 > N_3 > N_2 \gg N_1$ and with the number of linking C-atoms: $C_2 > C_3 \gg C_4$. Activity is usually higher for bridged and cyclic systems than for linear analogues. Examples of some N-based ligands used successfully in Cu-based ATRP are shown in Figure A.10.

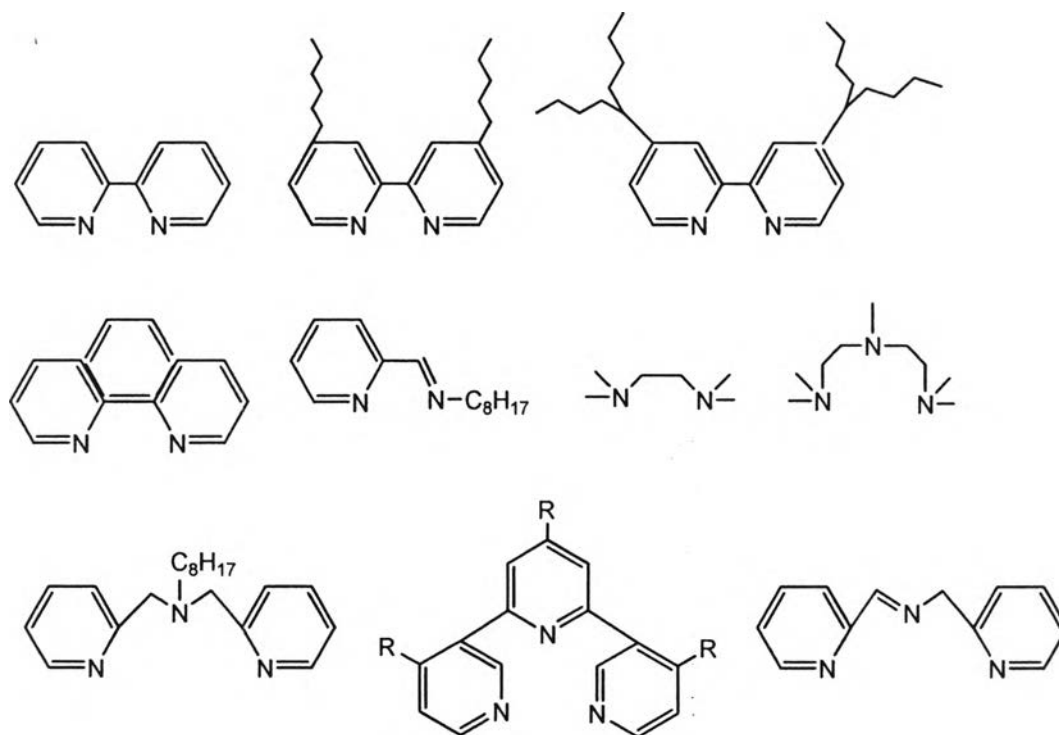


Figure A.10 Examples of ligands used in copper-mediated ATRP.

A.5 Solvent

Various solvents, such as benzene, toluene, anisole, diphenyl ether, ethyl acetate, acetone, dimethyl formamide (DMF), ethylene carbonate, alcohol, water, carbon dioxide, and many others, have been used for different monomers. A solvent is sometimes necessary, especially when the obtained polymer is insoluble in its monomer. In addition, interactions between solvent and the catalytic system should be considered. Catalyst poisoning by the solvent and solvent-assisted side reactions should be minimized (Matyjaszewski K. *et al.* 2001).

A.6 Temperature and reaction time

The rate of polymerization in ATRP increases with the increasing of temperature due to the increase of both the radical propagation rate constant and the atom transfer equilibrium constant. In general, the solubility of the catalyst increases at higher temperatures; however, catalyst decomposition may also occur with the temperature increase (Matyjaszewski K. *et al.* 2001).

EXPERIMENTAL

A.7 Equipment:

- | | |
|---------------------------------|------------------------------|
| 1. Reaction flasks | 2. Silicone oil bath |
| 3. Hot plate and stirrer | 4. Thermometer |
| 5. Distillation flask | 6. Condenser |
| 7. Syringes | 8. Glass and rubber stoppers |
| 9. Nitrogen gas | 10. Vacuum pump |
| 11. Temperature control machine | 12. Hose clamp |

A.8 Materials and Chemicals:

1. Butyl acrylate, BA (monomer for ATRP)
2. Acetone
3. Cellulose microcrystalline, CMF (Avicel)
4. Ethanol (95.5% purity)
5. 2-(Dimethylamine)-pyridine, DMAP (97% purity)
6. Triethylamine, TEA ($\geq 99.5\%$ purity, GC)
7. 2-Bromoisobutyl bromide, BIBB (98% purity)
8. 2,2'-bipyridyl, bpy ($\geq 99\%$ purity, NT)
9. N,N-Dimethylformamide, DMF ($\geq 98.0\%$ purity, GC)
10. Chloroform (anhydrous, $\geq 99.0\%$ purity)
11. Copper (I) bromide, CuBr ($\geq 98.0\%$ purity, RT)
12. Polypropylene, PP

A.9 Experiment Procedure

In-situ atom transfer radical polymerization on the surface of cellulose fibers experiment was set up by using butyl acrylate as a monomer, 2-Bromoisobutyl bromide (BIBB) treated fiber as an initiator, Copper (I) bromide (CuBr) as a catalyst, 2,2'-bipyridyl (bpy) as a ligand and N,N-Dimethylformamide (DMF) as a solvent. The experiment procedures are shown below:

A.9.1 An initiator preparation for ATRP (Figure A.11):

1. Mixed dry CMF and chloroform in the reaction flask then, injected DMAP and TEA.

2. Keep stirring at 0°C by using a saline as a coolant in the temperature controller for 10 minutes.

3. Prepared the BIBB solution by mixed BIBB and chloroform in beaker and added into the distillation flask which is connected to the reaction flask.

4. Purged nitrogen gas (one minute for each time) and vacuum (1–2 minutes or until it's no bubbles in the reaction flask for each time) for three times, so it's take 10–15 minutes.

5. Dropped BIBB solution into the reaction flask within 1 hour and keep reacting at 0°C for 24 hours.

6 Keep reacting at room temperature for 48 hours.

7. Filtered the product (CMF–Br) by using vacuum pump, washed with acetone and keep drying in the oven overnight.

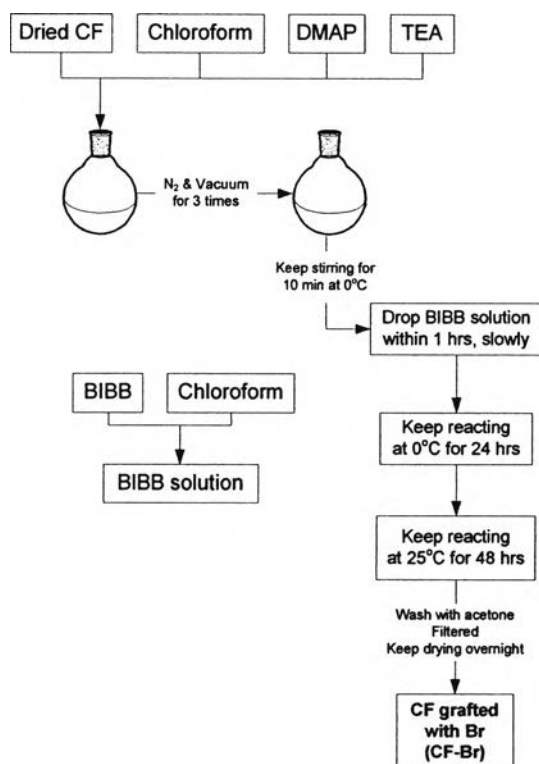


Figure A.11 The preparation of CMF initiator.

A.9.2 An ATRP reaction (Figure A.12):

1. Mixed dried CMF-Br, CuBr, bpy, and DMF in the reaction flask at room temperature for 10 minutes.
2. Purged nitrogen gas and vacuum for three times (same procedure with the preparation of the initiator).
3. Injected BA into the reaction flask.
4. Purged nitrogen gas and vacuum for three times again (same procedure with the preparation of the initiator).
5. Keep reacting at 70°C for 8 hours.
6. Filtered the product (CMF-PBA) by using vacuum pump, washed with ethanol and de-ionized water, and keep drying in the oven overnight.

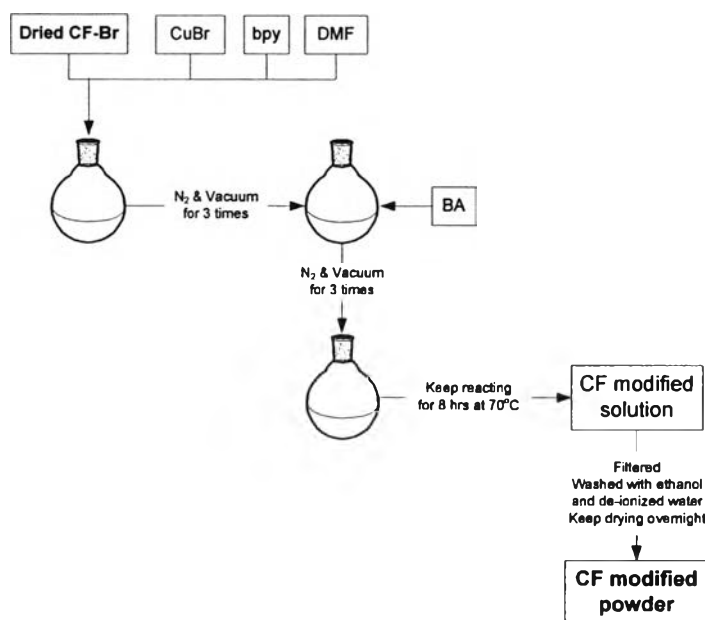


Figure A.12 An ATRP reaction of CMF.

RESULTS AND DISCUSSION

A.10 Preparation and Characterization of CMF-Br Initiator

In contrast to conventional radical polymerization, ATRP uses alkylhalogen compounds as initiators, such as the widely used 2-bromoisobutyrylate structures. For surface grafting by ATRP, a common way to functionalize the surface of matrix with the bromoisobutyrylate structure is to graft α -bromoisobutyryl bromide to hydroxyl group present on the surface (Luo N. *et al.* 2003; Carlmark A. *et al.* 2002). For CMF, the hydroxyl groups existing on the surface of CMF can be used to react with α -bromoisobutyryl bromide (BIBB) to form the macro-initiators. Figure A.13 shows the procedure of grafting BIBB onto the surface of CMF.

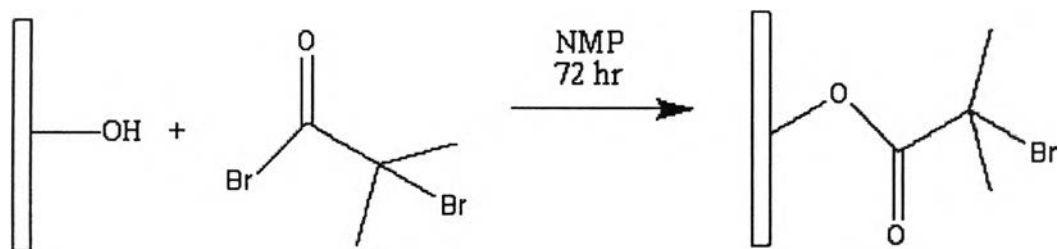


Figure A.13 Reaction procedure for preparing macro-initiator, CMF-Br.

Figure A.14 shows the FTIR spectra of CMF and purified CMF-Br. For the FTIR of CMF-Br, two new peaks were observed at 1738 cm^{-1} and 579 cm^{-1} , which were attributed to the stretching vibration of carbonyl groups and C-Br groups in BIBB compound, implying that BIBB was grafted onto the surface of CMF and bromoisobutyrylate groups were immobilized on the surface of CMF.

In order to achieve the amount of α -bromoisobutyryl bromide grafted onto the surface of CMF, thermogravimetric (TG) decomposition measurement was performed to quantify the amount of bromine. In Figure A.15, the thermogravimetric decomposition thermograms taken between 50 and 700°C for the CMF and CMF-Br are shown. For CMF, it is very clear to see only one sharp weight loss that has its inflection point at around 317°C , corresponding to the onset of decomposition, T_d , of CMF. However, in contrast, the first onset of decomposition of CMF-Br is found to

be lower at 230°C. Furthermore, CMF decomposed over a narrower temperature range, whereas CMF-Br over a wider range. The decrease in T_d and the wider range observed for CMF-Br are evidences of the presence of BIBB since the initial slight weight loss resulted from the degradation of BIBB, even though a literature reported a T_d of 270°C of BIBB grafted on carbon nanotubes.

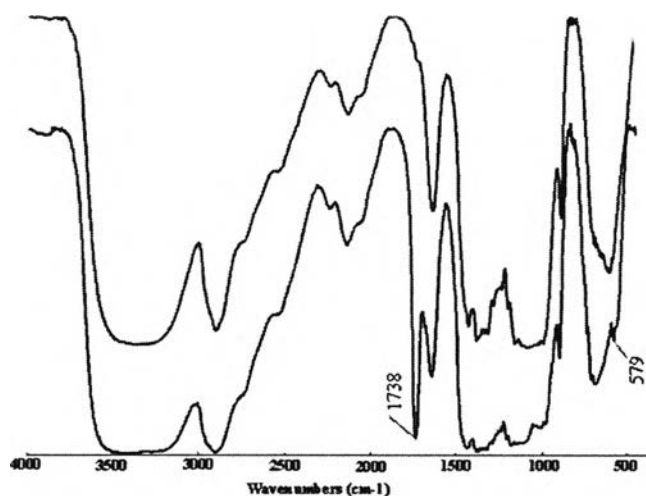


Figure A.14 FTIR spectra of CMF and CMF-Br.

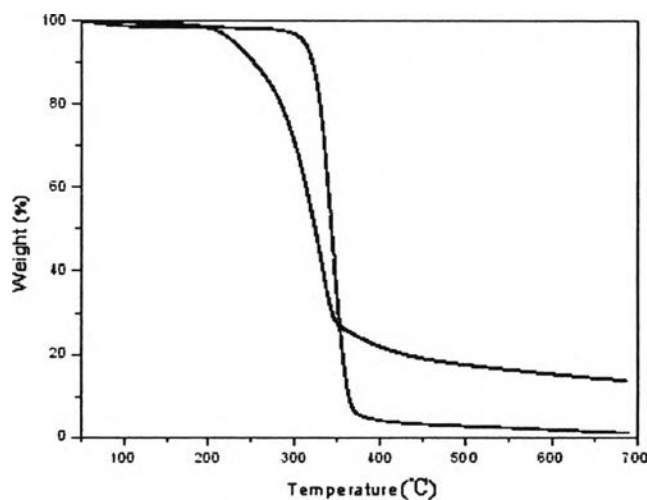


Figure A.15 TG curves of CMF and CMF-Br.

To show the detail of the decomposition of BIBB, derivative thermogravimetry (DTG) and TG curves of CMF-Br were shown in Figure A.16. The thermogram of CMF-Br contains three separate degradation steps with three maximum rate DTG peaks after 100°C. The third smaller decomposition peak, which appears around 375°C where CMF is completely decomposed, may result from the thermal degradation of a new crosslinked material formed by thermal crosslinking reactions occurring in initial stages of a degradation process. Crosslinking reactions during the thermal degradation of polymers have been reported for hydroxyl-terminated siloxanes, polyamides, and poly (3-hydroxybutyrate) where reactions between the terminal hydroxyl end groups on polymer chains and the carboxylic acid groups formed by chain scission were proposed. The maximum decomposition peak at 260°C is caused by the degradation of CMF, and the decrease of T_d is affected by the substitution of CMF hydroxyls with BIBB. This result is in correspondence with the report of Bikales N. M. *et al.* (1971). Therefore, the thermal stability of CMF-Br is lower than that of original CMF. What needs to be notice is the first smaller decomposition peak at 230°C, which results from the degradation of BIBB grafted on CMF with a content of 11.7%. Therefore, we can get the molar amount of 0.0008mol of Br in 1g CMF-Br. These results obtained from TGA are listed in Table A.2.

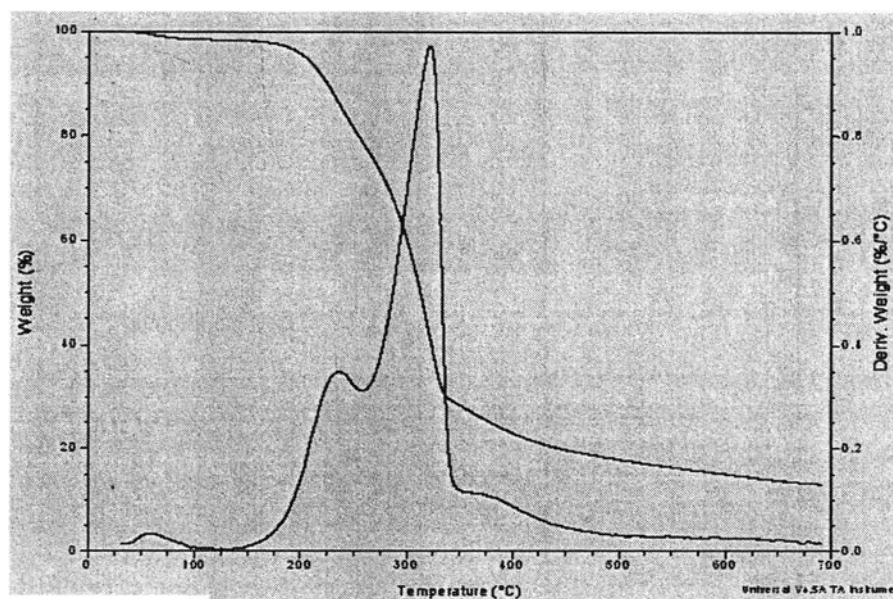


Figure A.16 TG and DTG curves of CMF-Br.

A.11 Graft Polymerization and Characterization of CMF-PBA

The polymerization of BA with CuCl/PMDETA as the catalyst and CMF-Br as the initiator was carried out in toluene solvent at 95 °C for 24 hours. Two samples, CMF-PBA-1 and CMF-PBA-2, were prepared using the same macro-initiators. The target polymerization degrees of the two samples were predetermined as 10 and 15 respectively according to the molar amount of Br in CMF-Br. The reaction procedure is shown in Figure A.17.

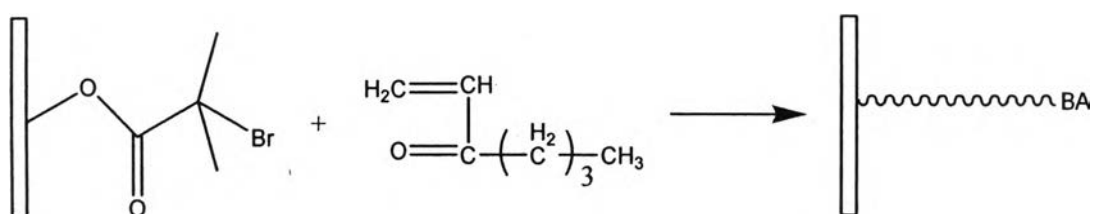


Figure A.17 Reaction procedure for preparing CMF-PBA.

Figure A.18 shows the FTIR of original CMF and the CMF-PBA sample. As a result of polymerization in situ of ATRP, a new absorption band appears at 1738 cm^{-1} , which can be attributed to the stretching vibration of carbonyl groups in PBA. Furthermore, the peak intensity around 2900 cm^{-1} was increased due to the addition of CH_2 and CH_3 groups to CMF. It was also found that the strong absorption at 1640 cm^{-1} was decreased that is ascribed to intermolecular H-O-H stretching, indicating that a decrease in H-O-H interactions when the PBA macromolecules were introduced onto the surface of CMF. Therefore, by the comparison of FTIR between CMF and CMF-PBA, it can be confirmed that PBA was graft polymerized onto the surface of CMF.

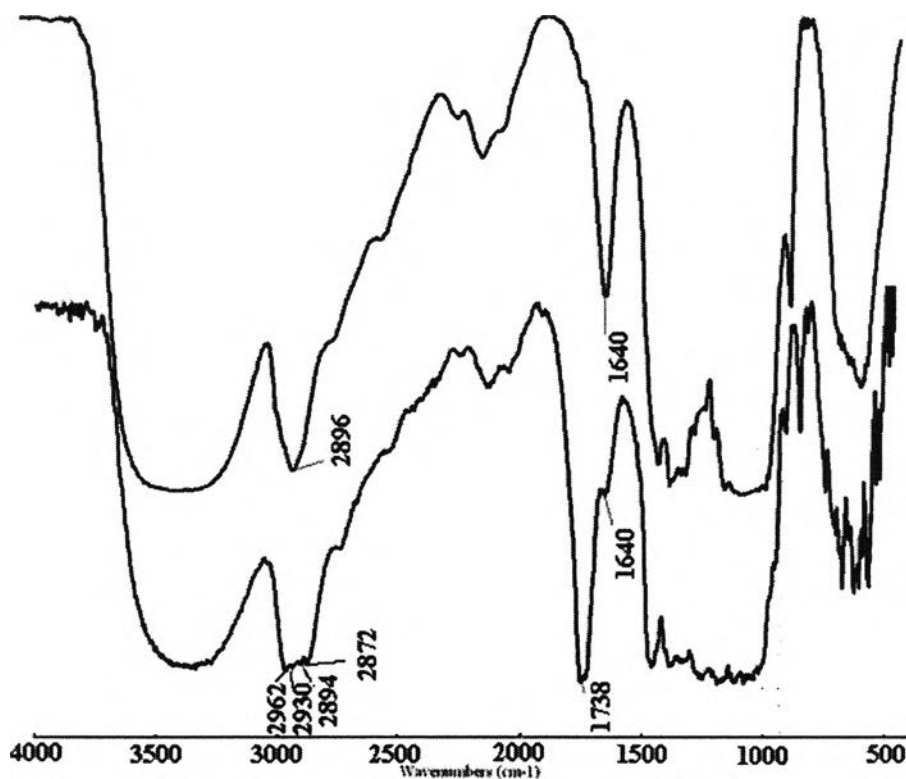


Figure A.18 FTIR spectra of CMF and CMF-PBA.

Thermogravimetric curves for CMF, CMF-PBA-1 and CMF-PBA-2 were shown in Figure A.19 and the data were summarized in Table A.2. From Table A.2, it can be seen that CMF-PBA-2 processes a higher content of PBA in comparison with CMF-PBA-1, indicating that the chains of PBA on CMF-PBA-2 is longer than that of CMF-PBA-1. Compared with the T_d of CMF at 317°C from Table A.2, the initial weight loss of CMF-PBA-2, which was resulted from the decomposition of CMF, was increased to 328°C because the introduction of longer PBA macromolecules chains increases the stability of CMF-PBA. Also, the second sharp inflection related to the weight loss of PBA at 390°C was higher than that of CMF-PBA-1 due to the longer PBA chains. However, for CMF-PBA-1, the contrary effect was observed. Its curve deviated from the baseline at 230°C which is in correspondence to the T_d of BIBB, even though not detected for CMF-PBA-2 due to the relative lower content of BIBB. Furthermore, the breaking point of CMF-PBA-1 took place at 311°C which is lower than that of CMF, implying that the stability of modified CMF

was decreased due to the introduction of shorter polymer chains. Compared with TGA plots in Figure A.16, weight loss of thermal crosslinking reaction was not observed for all three samples.

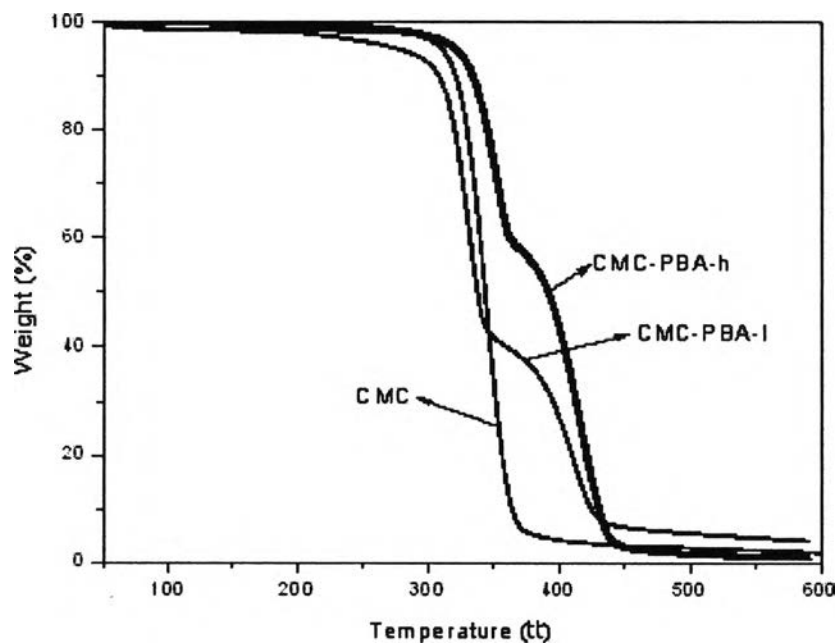


Figure A.19 TG curves of CMF, CMF-PBA-l and CMF-PBA-h.

Table A.2 Thermostability and contact angle results of CMF, CMF-PBA-l and CMF-PBA-h

Sample	PBA Content (%)	T _d of CMF (°C)	T _d of PBA (°C)	Contact angle (degree, °)
CMF	-	317	-	0
CMF-Br	-	258.7	-	-
CMF-PBA-1	47%	311	388	112.8
CMF-PBA-2	58%	329	393	112.5

A.12 The Controllability of BA Graft Polymerization

To study the possibility to control the length of the grafts on the surface of CMF, The GPC analysis of the polymers obtained from the hydrolysis of CMF-PBA-1 and CMF-PBA-2 were performed. Figure A.20 shows two main peaks of the two cleaved-off polymers. For CMF-PBA-1, a narrow and mono-modal peak is observed; however, CMF-PBA-2 shows a broadening peak with a small shoulder at shorter elution times, implying that the loss of bromine during the reaction once increasing the chains length. The results of molecular weight and distribution obtained by GPC measurements are list in Table A.3.

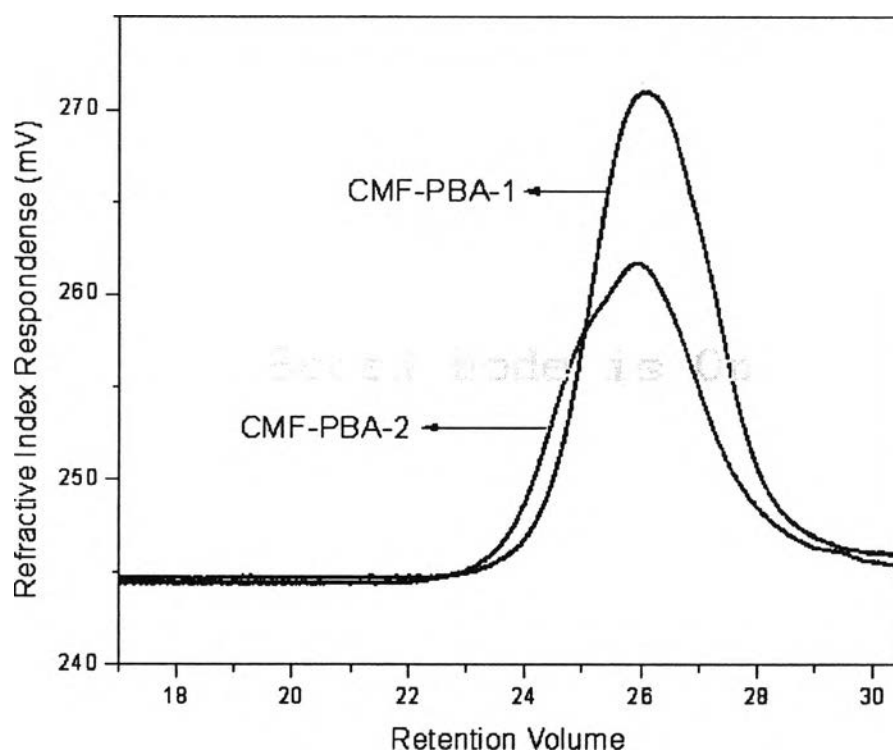


Figure A.20 GPC traces of the polymers cleaved-off from CMF-PBA-1 and CMF-PBA-2 prepared using the same macro-initiator.

In addition, by the content of PBA grafted on CMF achieved from the results of TGA shown in Table A.2, the calculated molecular weight can be obtained, which is also shown in Table A.3. As shown in Table A.3, compared with the theoretical

values of M_n for the two samples, the experimental and calculated values decrease, which is in correspondence with the fact that the conversion of BA cannot be increased continuously with the reaction time increasing. Furthermore, for the two samples, the experimental values of M_n are close to the calculated values, especially for CMF-PBA-1, implying that the side reactions are neglectable and the polymerizations are controllable with polydispersity indices (PDI) down to 1.4.

Table A.3 GPC results and calculated values from the results of TGA

Samples	Aimed DP	Theoretical M_n	Experimental M_n	Calculated DP	PDI
CMP-PBA-1	10	1280	1050	1108	1.41
CMP-PBA-2	15	1920	1810	1726	1.86

A.13 Hydrophobicity Characterization of CMF-PBA

The hydrophobicity of modified CMF is very important for increasing the dispersion of the dispersion of CMF in PP matrix. The hydrophobicity of CMF-PBA samples was investigated by measuring the water contact angle. The contact angle measurements are shown in Figure A.21 and the data are summarized in Table A.2. From Figure A.21, it is very clear that the contact angles of CMF-PBA-1 and CMF-PBA-2 are increased to a great extent in comparison with that of original CMF, on which water droplet will be absorbed immediately once it contacts the surface due to its strong hydrophilicity. Furthermore, the contact angle of CMF-PBA-1 is almost the same with that of CMF-PBA-2. The results suggest that the surface of CMF-PBA-1 was covered completely by PBA; therefore, for CMF-PBA-2, the film thickness of PBA grafted on CMF increases with the aimed DP of PBA increasing, which is given an evidence of living polymerization for our reaction systems.

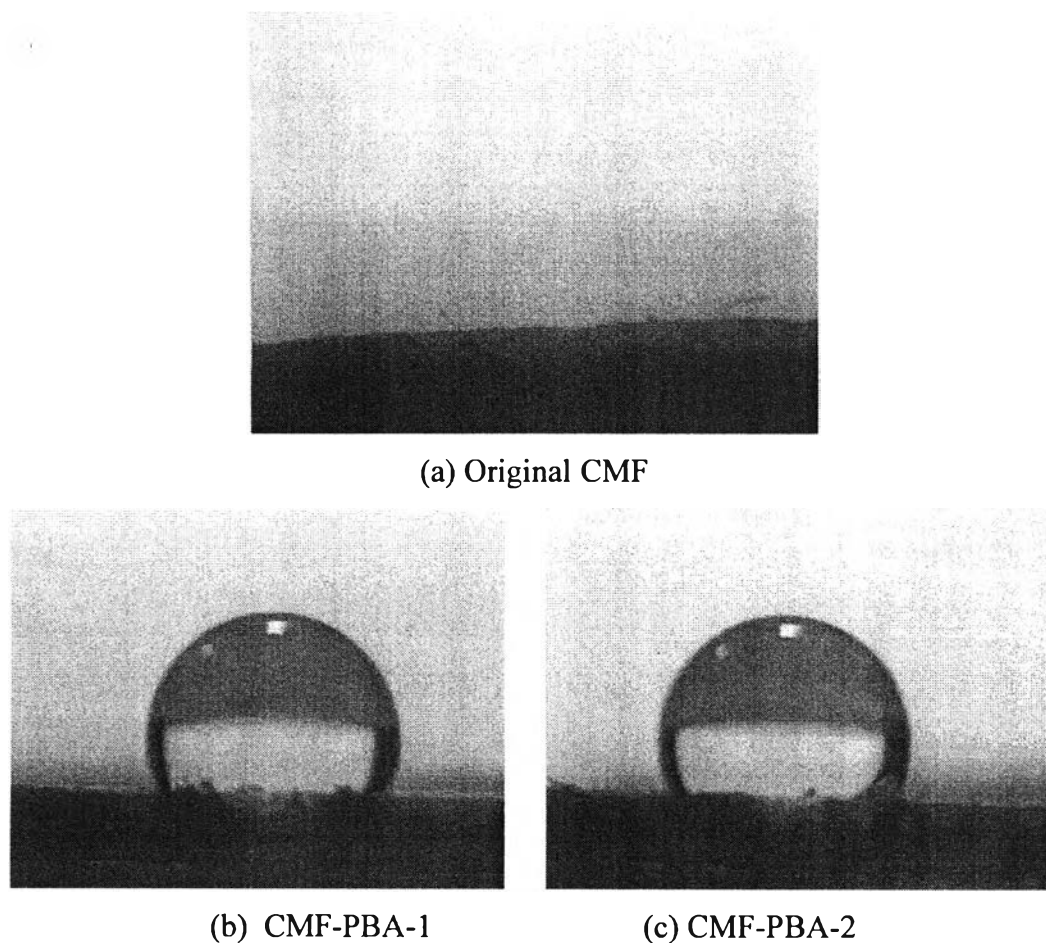


Figure A.21 Contact angle of CMF, CMF-PBA-1 and CMF-PBA-1.

SEM was used to characterize CMF and modified CMF samples. Figure A.22 shows the SEM images of unmodified CMF and modified CMF, CMF-PBA-1 and CMF-PBA-2. From the image of CMF-PBA-2 (Figure A.22 (b)), it can be seen that some CMF powders were crosslinked due to the couple termination reactions, which was resulted from the longer reaction time. This is in accord with the broadening distribution and the appearance of the shoulder in the GPC results. Furthermore, the surface of CMF-PBA-1 became smoother in comparison with that of CMF. On the other hand, the SEM micrographs provide a evidence of rough surface for CMF (Figure A.21 (a) and (c)). However, after grafted by PBA using the controlled ATRP, it can be observed clearly that the surface of CMF-PBA-1 is even and smooth and some holes on the surface of CMF were covered completely by grafted PBA. More-

over, the appearance of single CMF shows that the couple termination reactions are neglectable due to the controlled polymerization.

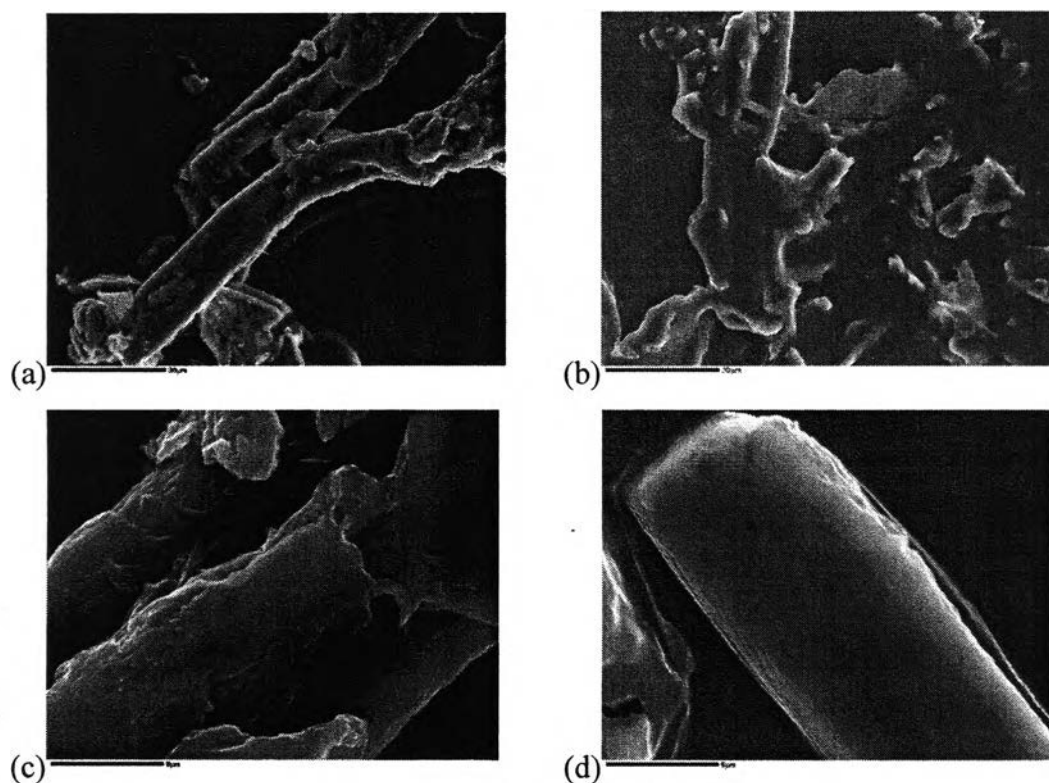


Figure A.22 SEM images of the surface of CMF and modified CMF; (a) SEM image of CMF, (b) SEM image of CMF-PBA-2, (c) SEM image of CMF and (d) SEM image of CMF-PBA-1

A.14 Dispersity and Compatibility in PP Matrix

Figure A.23 shows the dispersion of CMF-PBA in PP matrix using LM under UV light. In Figure A.23, CMF-PBA fluoresce by the excitation of UV at 488nm, leading to evident difference from PP matrix. As shown in Figure A.23, CMF-PBA-1 is evenly dispersed in PP matrix and the individual CMF is observed, implying the increase of the dispersion in PP matrix. Furthermore, a tendency of orientation resulted from the shear flow in twin-screw extruder is evident from the LM measurement, causing a continuous contribution in PP matrix.

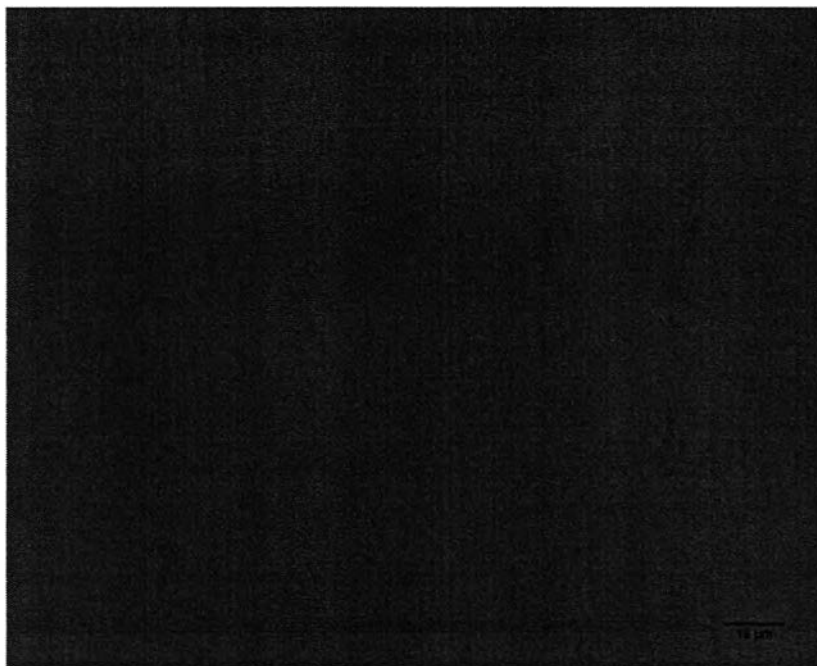


Figure A.23 Light Microscope (LM) images under UV light of the sections of CMF-PBA-1 in PP matrix.

As seen in Figure A.23 it is difficult to clearly observe the interfaces between CMF-PBA-1 and PP matrix, and therefore an estimate of the compatibility is not obtained. SEM analysis of the biocomposites showed to be a good alternative to electron microscopy. Figure A.24 shows the SEM images of CMF, CMF-PBA and CMF-18OH, thereof, CMF-18OH was the modified CMF grafted with octadecyl alcohol that was prepared by our group previously. In Figure A.24 (a), it is clear that the unmodified CMF separates from the PP matrix and the interface between the surface of CMF and PP matrix is so evident due to the hydrophobicity of CMF. In contrast, the interface between the surface of the CMF-18OH and PP matrix was not observed, implying that the CMF-18OH with some shorter organic chains shows better compatibility than CMF. On the other hand, from Figure A.24 (b), it can be seen that the CMF-18OH is pulled out of the PP matrix and some parts of the CMF-18OH stand out, which indicates that the octadecyl alcohol organic chains are too short to adhere to the PP matrix. However, in Figure A.24 (c), using longer PBA chains as the grafts on CMF, the compatibility with PP became so good that CMF-PBA was integrated with PP matrix and broke together with PP when the composite was brittle ruptured

by liquid nitrogen. In Figure A.24 (c), the interface between CMF-PBA-1 and PP is not observed and the outshoot of CMF-PBA are not observed, even the two phases of CMF-PBA-1 and PP are difficult to discern unless the vicinity of CMF is surrounded by a spot of residual dark Cu complex.

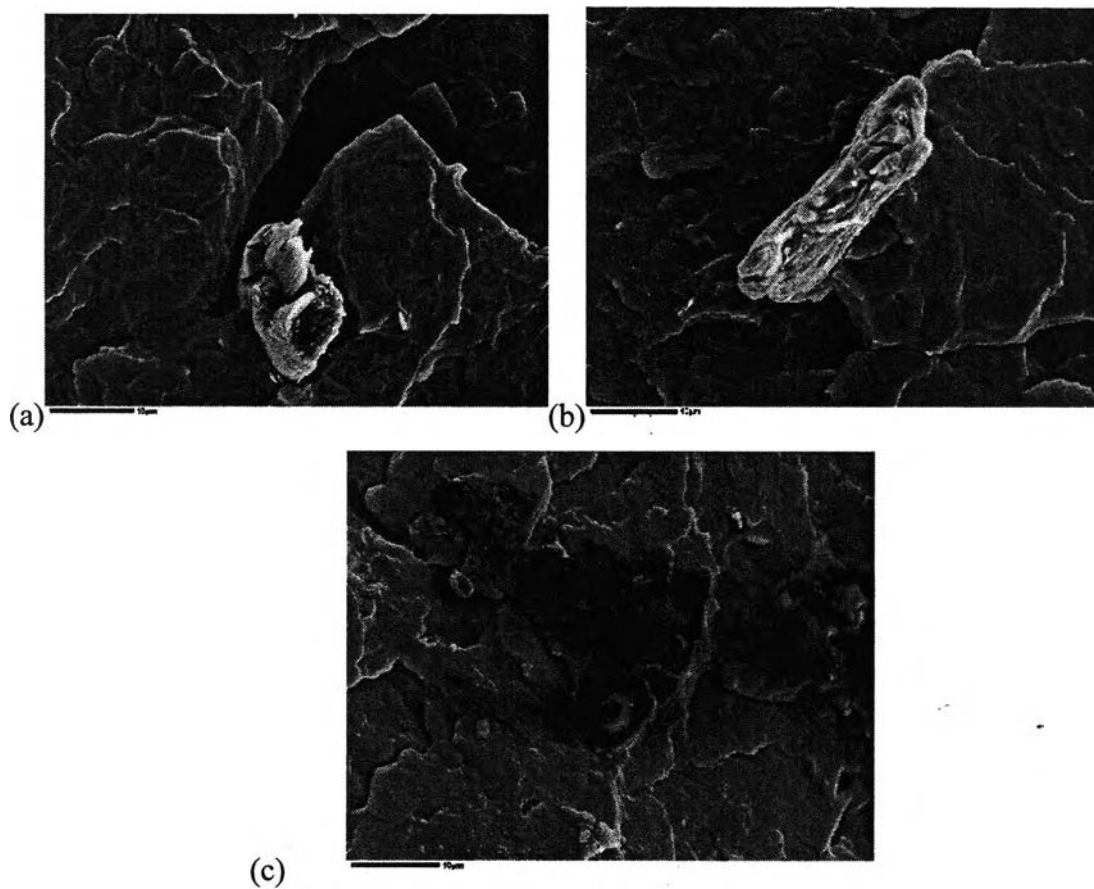


Figure A.24 SEM images of the ruptured surface of CMF and modified CMF samples in PP matrix.

CONCLUSIONS

In this study, CMF-Br obtained by esterification of hydroxyl groups on CMF with BIBB was used as a macro-initiator. Furthermore, the presence of Br was characterized and quantified by FTIR and TGA measurements, which helps to predetermine the molecular weight and distribution of butyl acrylate. The modified CMF was then grafted with butyl acrylate using ATRP, targeting different DPs of the grafts. The grafted CMF was analyzed with FTIR, which showed the presence of PBA on the surface of CMF. The characterization of TGA and GPC indicated that the graft polymerization on CMF for our reaction system is controlled. The polydispersities of two modified samples, CMF-PBA-1 and CMF-PBA-2, were low and the experimental molecular weights of them were close to the predetermined value. However, for CMF-PBA-2 with longer PBA chains, the GPC results showed that couple termination reactions took place during the longer reaction time, which was further confirmed by the SEM analysis due to the presence of some crosslinked CMF. Water contact angle showed that the hydrophobicity of the modified samples increased. As a result of modification, the LM and SEM analysis showed the dispersion and compatibility of PP-GMA-1 in PP matrix were evidently increased.

APPENDIX B

Enhancement of the Paper Performance

During the time for waiting the chemicals and blending PP/modified-fibers process, I had a chance to study the paper making process to enhance the paper properties by using the hydrophobic–modified cellulose microfibrils, products from ATRP and grafting technique, as enhancement agent.

Since the modified cellulose microfibrils are highly hydrophobic property, to change this hydrophobic to hydrophilic surface of the modified cellulose microfibrils. Many types of surfactant were used including Polyoxyethylene, Catasorb, Sodium oleate, Dodecyltrimethylammonium bromide, Tetrabutylammonium iodine, Stearic acid and Cetyltrimethylammonium bromide. Catasorb, a wetting agent with good affinity for cellulose fibers in the wet–end of a paper machine, was obtained a good compatibility with the modified cellulose microfibrils by vary at 1 wt% and 10 wt%.

The amount of the modified cellulose microfibrils used was 2 wt% based on the amount of pulp. Table B.1 summarize the samples that had to prepare for the enhancement of the paper performance.

Table B.1 The samples preparation for the enhancement of the paper performance

Sample	Surfactant (%)
2% CMF–C ₁₈ OH (Grafting)	10
	1
2% CMF–PBA (ATRP)	10
	1

Figure B.1 shows the flow chart of paper making process. The specific amount of pulp was calculated in order to make 10 handsheets.

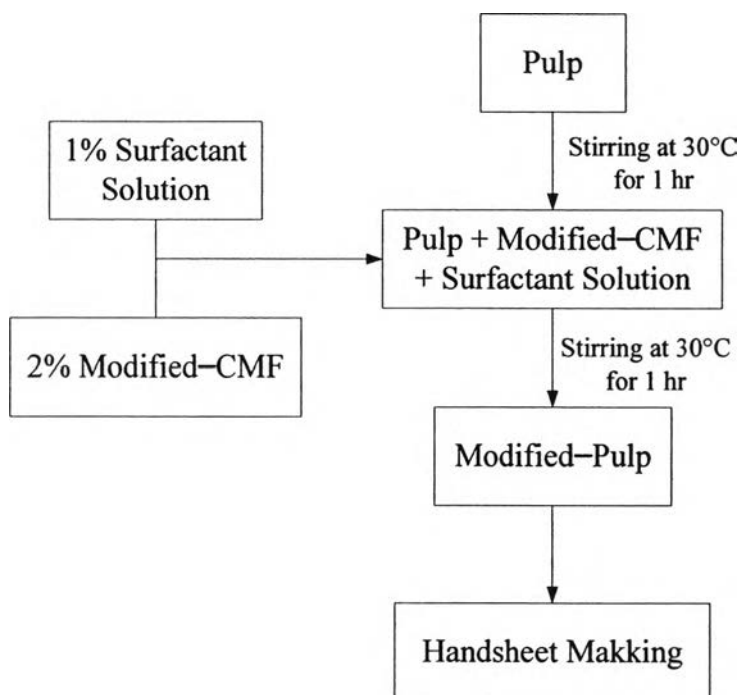


Figure B.1 Paper making flow chart.

All physical properties of paper were tested including tensile strength, brightness and porosity, thickness, tearing, bursting and water retention value. The results are shown in Table B.2.

Table B.2 Physical properties of modified-paper

Sample	Strength (Nm/g)	Burst (mN)	Tearing (mN)	WRV
Blank	32.34	2.085	26.56	1.1507
CMF-18OH	28.24	2.153	25.30	1.1011
CMF-PBA	26.80	2.157	18.43	1.0603

Table B.2 (cont') Physical properties of modified-paper

Sample	Scat Coefficient	Apparent Density(kg/m ³)
Blank	32.23	63.9
CMF-18OH	33.58	66.7
CMF-PBA	33.42	78.4

The thickness results are similarly in all three samples. The water retention value which indicated the hydrophobicity of paper, increased for the modified-papers meaning that the modified-papers are more hydrophilic characteristic (unexpected results).

Tensile strength refers to fiber-fiber bonding in the modified-paper, the lower number obtained a softer of paper which benefit for tissue paper application. Also for the tearing strength, this property shows how easy to tear or rip the paper. The scattering coefficient represents the porosity of paper which is not much different in this case.

Figure B.2-B.7 show the paper making instrument.

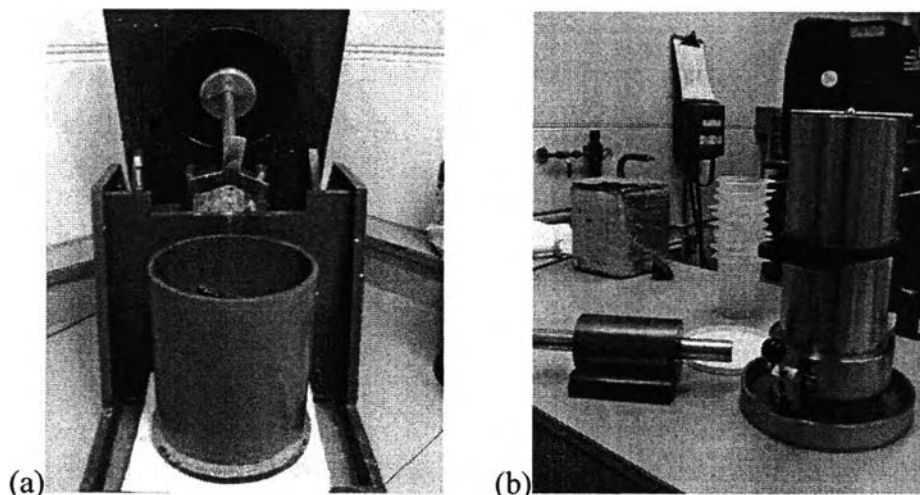


Figure B.2 (a) Aggregator and (b) filter.

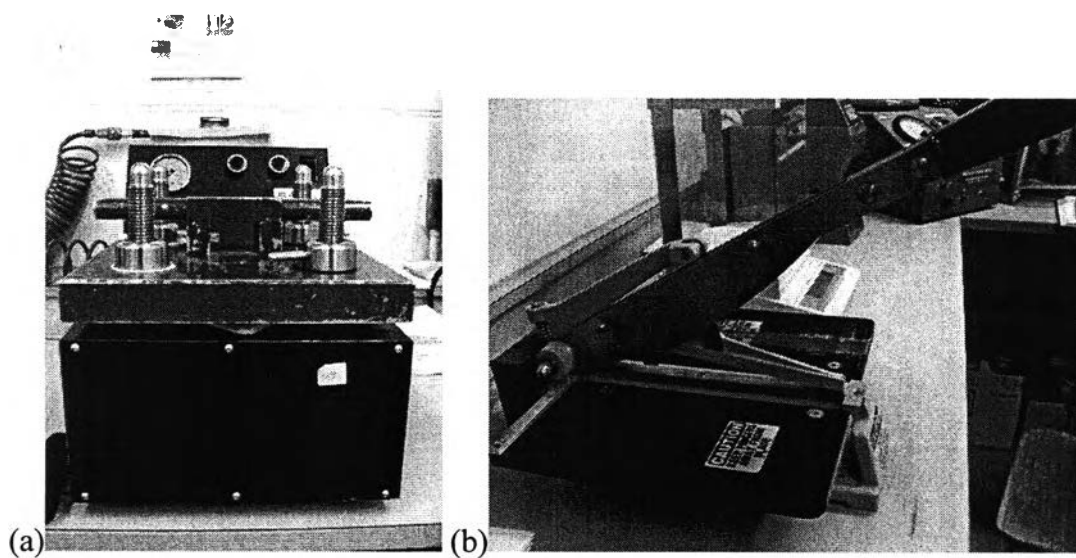


Figure B.3 (a) Compress system and (b) cutting equipment.

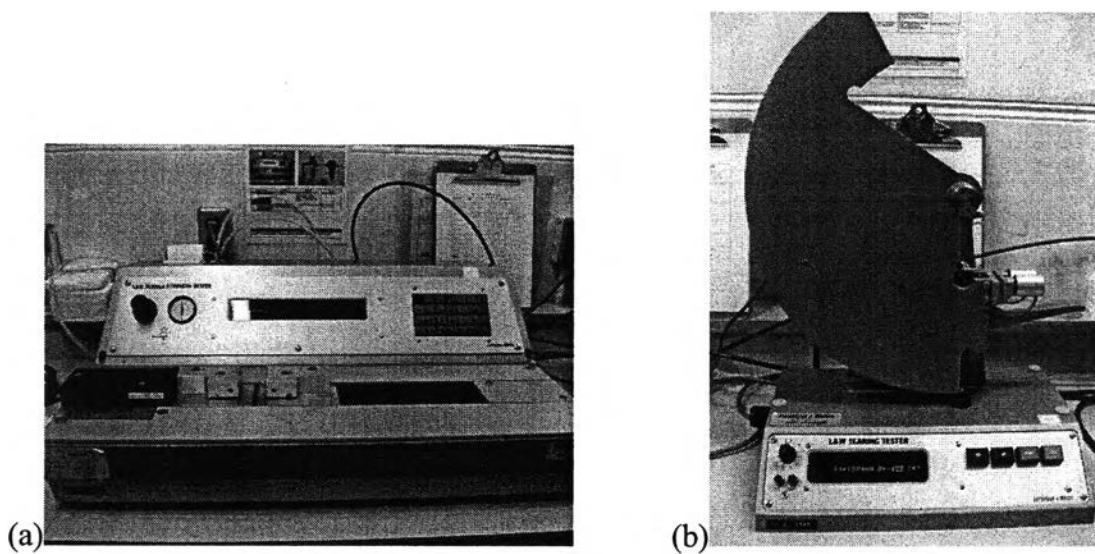


Figure B.4 (a) Tensile strength and (b) tearing strength equipment.

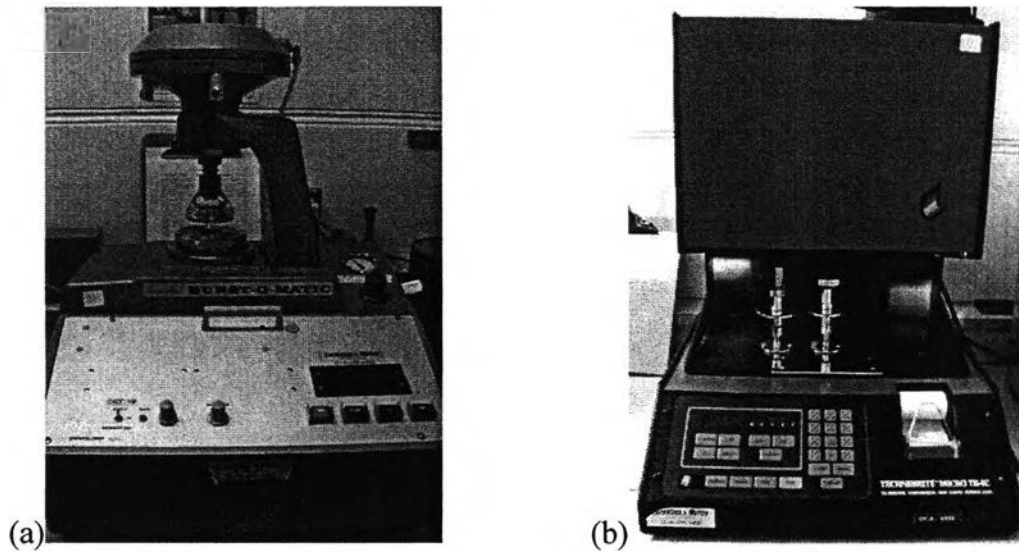


Figure B.5 (a) Bust strength and (b) brightness equipment.

APPENDIX C

BET Results of CMF and modified-CMF

Table C.1 BET Results of CMF and modified-CMF

Sample	$a_{s,BET}$ (m²/g)	Total pore volume (cm³/g)	Mean pore diameter (nm)
Blank	0.73098	5.6773E-03	31.066
TDI+18OH Grafted CMF_5%	2.20660	8.5506E-03	15.500
TDI+CMF Grafted 18OH_5%	1.47590	7.4680E-03	20.239

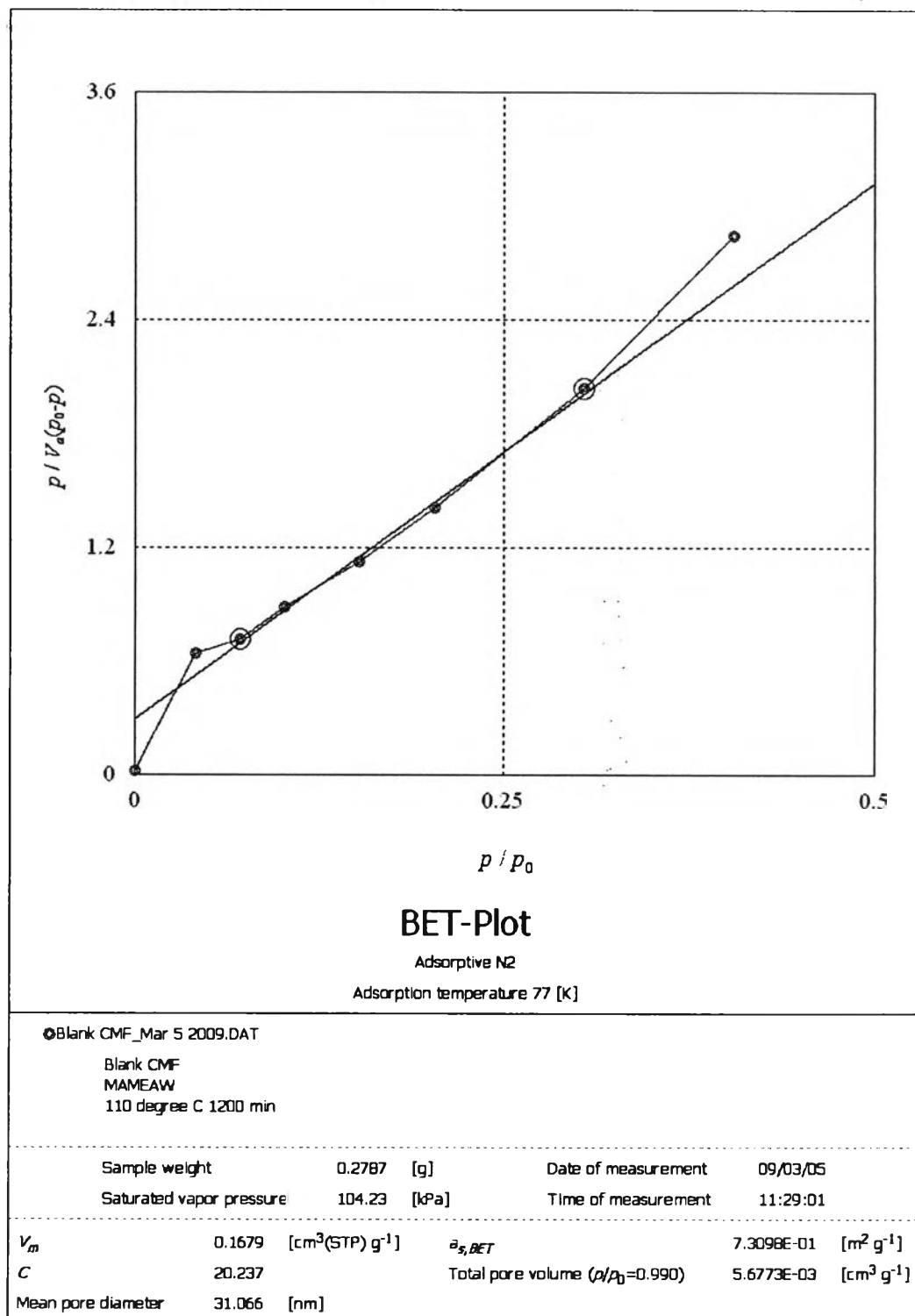


Figure C.1 BET plot of CMF (Blank) sample.

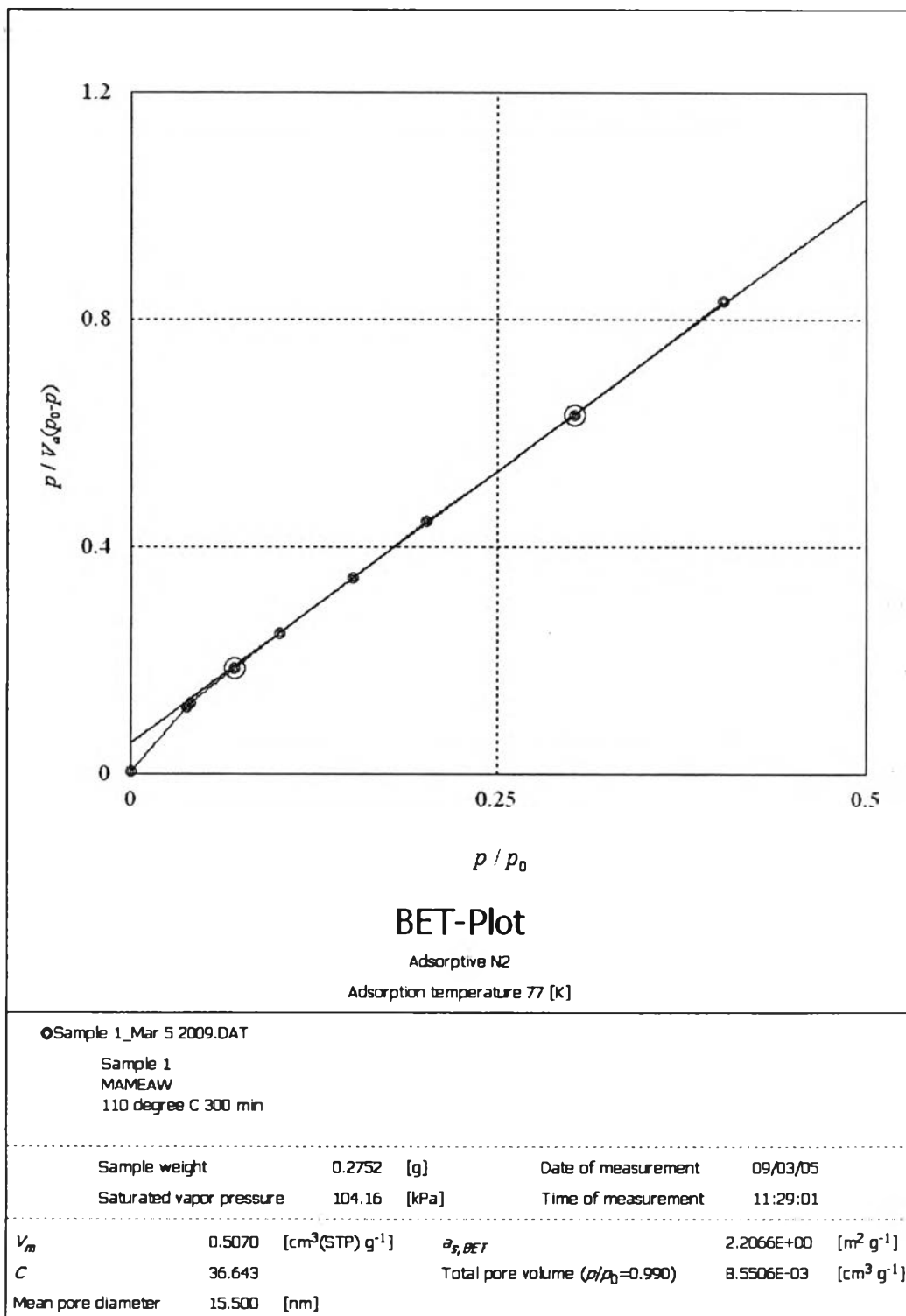


Figure C.2 BET plot of TDI+18OH Grafted CMF_5% sample.

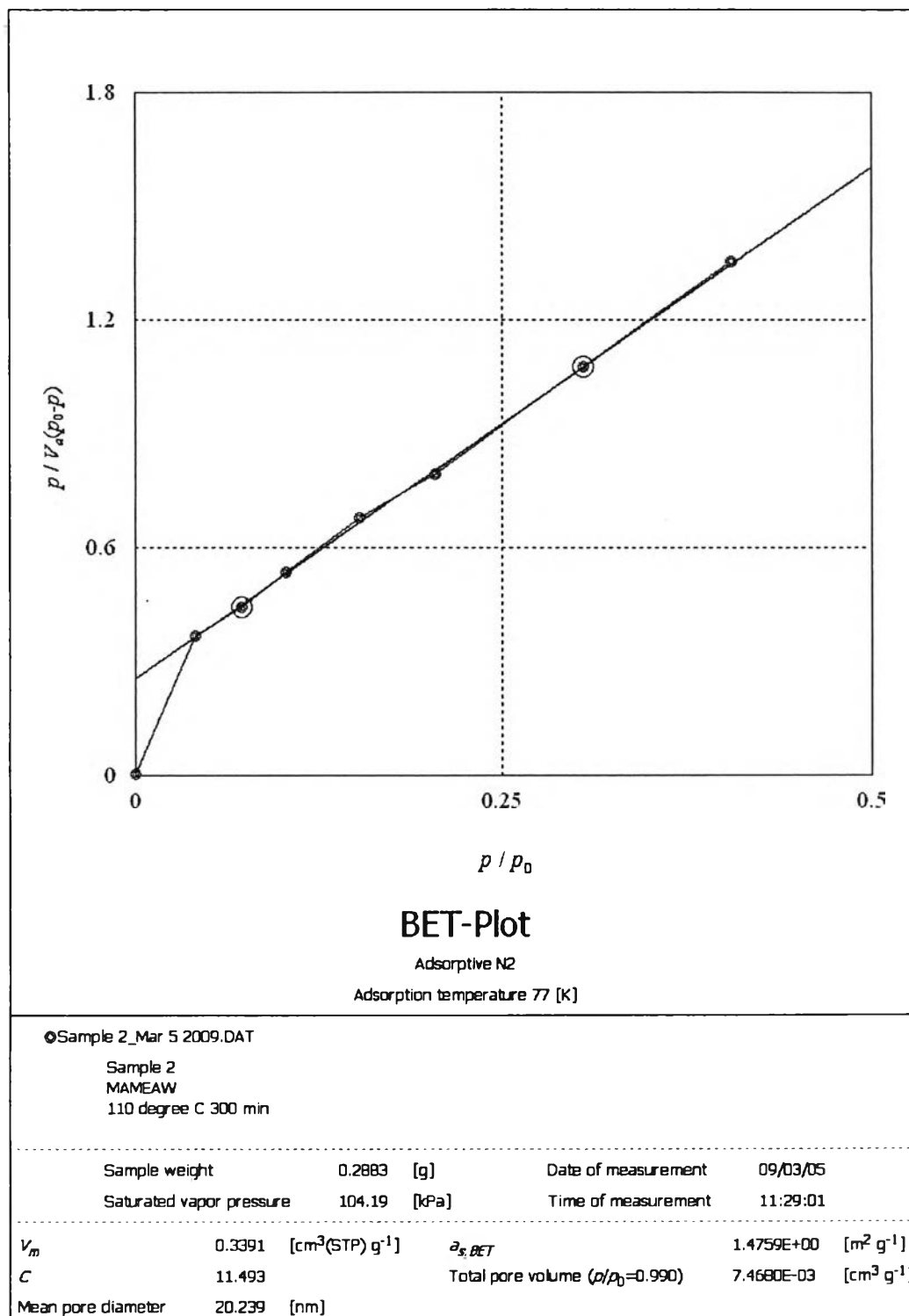


Figure C.3 BET plot of TDI+18OH Grafted CMF_5% sample.

CURRICULUM VITAE

Name: Ms. Wilailak Chanklin

Date of Birth: March 13, 1985

Nationality: Thai

University Education:

2003–2007 Bachelor Degree of Engineering in Chemical Engineering,
Faculty of Engineering, Burapha University, Chonburi,
Thailand.

Work Experience:

2006 Position: Student internship as process engineer

Company name: ESSO (Thailand) Public Company Limited

Study Experience:

2008 Position: HQP (High Quality Personnel) student

Academic Institute: AUTO21 2008 Conference

Published Work

2009 Chanklin, W., Li, S., and Xiao, H. (2009) Hydrophobic-Modified Cellulose Fibers and Cellulose Microfibrils as Reinforcements for Biocomposites. Society of Plastics Engineers Annual Technical Conference 2009.

